SUPPLEMENTARY INFORMATION

Long-term Variability in Black Carbon Emissions Constrained by Gap-filled Absorption Aerosol Optical Depth and Associated Premature Mortality in China

Wenxin Zhao[1], Yu Zhao[1,2*], Yu Zheng[3], Dong Chen[4], Jinyuan Xin[5], Kaitao Li[6], Huizheng Che[3], Zhengqiang Li[7], Mingrui Ma[1], Yun Hang[8]

1 State Key Laboratory of Pollution Control and Resource Reuse, School of Environment, Nanjing University, 163 Xianlin Rd., Nanjing, Jiangsu 210023, China

2 Jiangsu Collaborative Innovation Center of Atmospheric Environment and Equipment Technology (CICAEET), Nanjing University of Information Science and Technology, Jiangsu 210044, China

3 State Key Laboratory of Severe Weather (LASW) & Key Laboratory of Atmospheric Chemistry of CMA (LAC), Chinese Academy of Meteorological Sciences, Beijing 100081, China

4 Jiangsu Provincial Academy of Environmental Science, 176 North Jiangdong Rd., Nanjing, Jiangsu 210036, China

5 LAPC, Institute of Atmospheric Physics, Chinese Academy of Sciences, Beijing 100029, China

6 School of Information, Space Engineering University, Beijing 101416, China

7 State Environmental Protection Key Laboratory of Satellite Remote Sensing, Aerospace Information Research Institute, Chinese Academy of Sciences, Beijing 100101, China

8 Gangarosa Department of Environment Health, Rollins School of Public Health, Emory University, 1518 Clifton Road NE, Atlanta, GA 30322, USA

*Corresponding author: Yu Zhao

Phone: 86-25-89680650; email: *yuzhao@nju.edu.cn*

Contents of this file

Number of pages: 66

Number of texts: 4

Number of tables: 13

Number of figures: 10

Table of Contents

Text sections

Text S1 Description of XGBoost model and specific feature selection

XGBoost model description

The XGBoost algorithm is an additive model based on hundreds of decision tree models. XGBoost first builds multiple CART (Classification and Regression Trees) models to predict the data set, and then integrates these trees as a new tree model (Liu et al., 2021). The model will continue to iteratively improve, and the new tree model generated in each iteration will fit the residual of the previous tree. As the number of trees increases, the complexity of the ensemble model will gradually increase until it approaches the complexity of the data itself, at which point the training achieves the best results. XGBoost model has been widely used in predicting air pollution abundance and shown to outperform various statistical and machine learning models (Xiao et al., 2018a). Besides, XGBoost requires less training and predicting time than other machine learning techniques, i.e., random forest.

Specific feature selection

The selection of the specific features was based on the following basis. Firstly, according to various previous studies, meteorology, geography and temporal parameters were commonly taken as features for gap-filling of satellite product (Liang et al., 2020; Ma et al., 2022). To fill OMI AAOD in this study, we chose aerosol optical and meteorological parameters to reflect the optical properties, transport and diffusion of pollutants. Land-use data and elevation are ancillary variables which directly linked to emission sources and the pollution transport conditions. Considering the continuity in space and time, we also added temporal, latitude and longitude parameters to fill the data gap. Secondly, based on the "skimr" and "DataExplorer" packages in R software (version 4.1.2, https://www.R-project.org/), we went through the data distribution and examined the multicollinearity for selected features before model training. We deleted highly correlated features according to variance inflation factor (VIF) analysis to prevent the biased estimation and improve model efficiency. Thirdly, we trained multiple models with different combinations of model parameters and specific features, and determined the optimal feature group based on root mean squared prediction error (RMSE) minimization. The model parameters "*max_depth*" (maximum number of times for regression tree splitting) and "*colsample_bytree*" (proportion of interpretation features sampled for splitting at each node) provide an opportunity to randomly select

features for additive model training, and they were respectively determined at 6 and 0.4 to train our model. Not all interpretation features participate in the process of node splitting; thus, the possibility of random combination of model features is further improved.

Through above feature selection process, we determined the optimal feature combination and gap-filling model, to achieve best model performance. Changing the feature combination and parameterization of XGBoost may reduce the model performance and efficiency. Finally, to determine the key characteristics, we used the "xgb.importance" faction to assess the importance levels of specific features in three metrics, i.e., Gain is the average gain of splits which use the feature; Cover is the average coverage of splits which use the feature and the coverage is defined as the number of samples affected by the split; and Frequency is the frequency a feature appears in a tree.

Text S2 Description of CMAQ model setting and the prior emissions

The meteorology field input was provided by the Weather Research and Forecasting Model (WRF) version 3.9. We used a grid system at a horizontal resolution of 27×27 km covering the study domain (Supplementary Figure S1) in Lambert projection with two true latitudes of 40°N and 25°N, and the origin of domain was set at 103°E, 37°N. CMAQ V5.1 adopts the Carbon Bond Mechanism (CB05) and AERO5 mechanisms as the gas-phase chemistry and aerosol module, respectively. The lifetime of BC is mainly influenced by wet and dry removal processes in the atmosphere. The CMAQ model assumed that all aerosol particles are internally mixed and the wet removal of aerosol is proportional to wet removal of sulfate (Binkowski and Roselle, 2003). And the CMAQ model has used the dry deposition scheme of Pleim and Ran (2011), which assumed that key processes of aerosol dry deposition including gravitational settling, Brownian diffusion, surface impaction, surface interception, and rebound are functions of particle diameter Dp. We used a spin-up time of 7 days for each month to reduce the impact of initial condition. Details of modeling setting can be found in our previous works (Yang et al., 2021).

The prior anthropogenic emissions were taken from the Multi-resolution Emission Inventory for China (MEIC, http://www.meicmodel.org; last access: 25 May 2022), and the prior open biomass burning emissions were taken from Global Fire Emissions Database version 4.1s (GFED V4.1s, https://www.geo.vu.nl/~gwerf/GFED/GFED4/; last access: 25 May 2022). MEIC is a uniform bottom-up emission inventory model that provides detailed estimates of anthropogenic emissions of air pollutants in China for a long time period with regular updates. It includes a series of improved emission models including unit-based emission inventories for power and industrial plants, a high-resolution county-level vehicle emission inventory, and a residential combustion emission inventory based on national-wide survey data. It takes full consideration of variation in activity level and emission factors based on local measurements and policy implementation in China. Those efforts help improving the quality of emission estimation.

Text S3 Description of emission inversion sensitivity tests.

To explore the uncertainty of the inversion system, we conducted four sensitivity tests, which respectively applied AAOD at another longer wavelength of 865 nm (Test 1), separated BC AAOD with different dust light-absorption contributions (Test 2), adjusted MAE according to ground measurements (Test 3), and adjusted simulated BC lifetime (Test 4). The test designs are briefly summarized in Table S4.

Test 1

Given that AAOD at 483nm is partly contributed by BrC, we conducted a sensitivity test (Test 1) with AAOD at another longer wavelength of 865 nm, at which the light absorption was seldom influenced by BrC.

Available satellite observation of AAOD was limited. Specifically, OMI AAOD was inverted in the ultraviolet-visible (UV) wavelengths (270-500 nm) while POLDER AAOD with wider wavelength range (443-1020 nm) provided poorer spatiotemporal coverage. We extrapolated the XGBoost-predicted OMI AAOD at 483 nm to 865 nm, based on the absorption Angström exponent (AAE) obtained from POLDER. Firstly, we estimated POLDER AAE with Eq. S1:

$$\mathrm{AAE}_{\lambda_1-\lambda_2,i,m,n} = -\frac{\ln[AAOD_{POLDER,\lambda_1,i,m,n}/AAOD_{POLDER,\lambda_2,i,m,n}]}{\ln[\lambda_1/\lambda_2]} \quad \text{(S1)}$$

where $AAOD_{POLDER}$ represents POLDER AAOD at different wavelength; λ_1 and λ_2 represent two wavelengths (here we chose 490 nm and 865 nm); *i* represents the number of grids; and *m* and *n* represent year and month, respectively.

Then we estimated the spatial distribution of POLDER AAE with Kriging interpolation for periods with POLDER observations (2005-2013). For years without POLDER observations, we extrapolated AAE according to its interannual trend within 2005-2013 from linear regression. Thus we obtained AAE dataset with complete spatiotemporal coverage (2000-2020).

Secondly, based on the AAE dataset, we extrapolated the XGBoost predicted OMI AAOD at 483 nm to AAOD at 865 nm with Eq. S2, based on the AAE dataset:

$$AAOD_{OMI,\lambda_2,i,m,n} = AAOD_{OMI,\lambda_1,i,m,n} \times e^{\ln[\lambda_1/\lambda_2]\times \mathrm{AAE}_{\lambda_1-\lambda_2,i,m,n}} \quad \text{(S2)}$$

where $AAOD_{OMI}$ represents OMI AAOD at different wavelength.

Considering the negligible light absorption of BrC at 865 nm, we separated the contributions of dust with MERRA-2 fractions, and obtained BC AAOD at 865 nm. Finally, based on the dataset above, we re-estimated the posterior BC emissions at 865 nm with the "top-down" approach, and compared the results with the base case.

Test 2

Besides BrC, retrievals of BC AAOD from the satellite total AAOD observations need to identify the contribution by mineral dust. There are few studies on observing dust AAOD, while great differences exist in simulated dust AAOD between atmospheric transport models.

In the base case, we adopted the BC contribution to total AAOD from MERRA-2 which considered the effects of dust and light-absorption organic carbon. MERRA-2 adopted wind-driven dust emissions and updated dust optical properties (Meng et al., 2010), and presented great agreement between MERRA-2 and OMI AAOD in dusty regions (Buchard et al., 2017). For mainland China, the multiyear average fraction of dust AAOD to AAOD was 29% during 2000-2020 (Figure S3a). The highest dust fraction mainly appeared in western sand-generating provinces, i.e., Xinjiang, Qinghai, Gansu and Inner Mongolia, and the average multiyear fraction of those provinces reaches 52%.

However, some studies suggested that MERRA-2 may overestimate the dust light-absorption contribution due to excessive local dust emissions and transport of Asian dust (Bakatsoula et al., 2023). To evaluate the uncertainty caused by adopting the dust AAOD fraction from one single model, we conducted a sensitivity Test 2, based on the dust AAOD fraction from another atmospheric composition reanalysis dataset produced by the Copernicus Atmosphere Monitoring Service (CAMS, https://ads.atmosphere.copernicus.eu/cdsapp#!/search?type=dataset; last accessed on 8 October 2023). The multiyear average fraction of dust AAOD to AAOD was 14% for CAMS during 2003-2017 (Figure S3b), much lower than that of MERRA-2. To avoid the influence from BrC, we adopted AAOD at the wavelength of 865 nm obtained in Test 1. We re-estimated the posterior BC emissions in 2000, 2010 and 2020 (2005 and 2015 were not involved to save computational resources and time).

Test 3

Given the limited ability of spatial extrapolation of the empirical BC light-absorption model, we conducted a sensitivity test (Test 3) with adjusted MAE based on available measurements (listed in Table S5).

Firstly, we compared the simulated MAE with available measurements from publicly published studies. The average MAE simulated with the posterior emissions is

10.23 m^2/g (converted to values at 483nm, the same below), much higher than the value of freshly emitted BC (8.48 m^2/g, Bond et al., 2013). The simulated MAE is smaller than corresponding measurements with an NMB of -19%. As a comparison, the average of MAE from multi-model simulations at the global scale was 27% smaller than the representative measurements (Gliß et al., 2021). CTMs adopted different representation for mixing of BC aerosols resulting in diverse estimates of MAE (Chen et al., 2017b). Considering spatiotemporal representation, as shown in Supplementary Table S6, the measured and simulated MAE present similar seasonal (higher in autumn and winter) and regional patterns (higher in SCB, YRD and PRD). Besides, the simulated MAE presented smaller regional heterogeneity than existing observations, attributed probably to the limited ability of spatial extrapolation of this empirical model. MAE in the key regions (with NMB ranging -22%~-15%) was more underestimated than that in other regions (with NMB of -11%) compared with observations.

Secondly, to explore the influence of MAE uncertainty on BC emission estimation, we adjusted the simulated MAE by region and season, based on the differences between the simulations and observations as shown in Table S6. With the adjusted MAE, we re-estimated the posterior BC emissions with the "top-down" approach and compared the results with the base case.

Test 4

BC is a well-acknowledged short-lived atmospheric species with an atmospheric lifetime of days to weeks. The chemical transport model reproduces atmospheric processes with simplified algorithm, leading to uncertainties on the simulation of BC lifetime and thereby on the estimation of its atmospheric column concentration and emission inversion.

To evaluate this uncertainty, we firstly calculated the lifetime as the ratio of BC column mass concentration to total BC deposition rates (Gliß et al., 2021). The annual average BC lifetime for mainland China was calculated at 4.7 days in the base case (Figure S4), within the simulated range of 3.8~11.4 days reported by previous studies (Bond et al., 2013), but smaller than the 14 models average of 5.5 days described in Gliß et al. (2021). We then added a sensitivity Test 4, in which the BC lifetime in CMAQ was adjusted to 5.5 days (the multi-model average level) by changing the wet and dry

removal rates of BC. The posterior BC emissions were then re-estimated for 2000, 2010 and 2020 (2005 and 2015 were not involved to save computational resources and time).

Text S4 Decomposing the contributions of emission and meteorological factors to the mortality due to BC exposure

To separate the contributions of emission and meteorological factors to the mortality due to BC exposure over the four 5-year intervals (2000-2005, 2005-2010, 2010-2015 and 2015-2020), we designed scenarios with fixed emission (*FE*) and meteorological conditions (*FM*) in CMAQ modeling, respectively (Supplementary Table S7). The posterior BC emissions in *FE* and the meteorological conditions in *FM* were fixed at the level of the first year of each interval. During interval *t0-t1*, the contribution of meteorological variation was estimated as the difference between simulated BC concentrations from *FE* in year *t1* and *BASE* in year *t0* (Eq. S3), and the contribution of emission variation as the difference between simulated BC concentrations from *FE* and *BASE* in year *t1* (Eq. S4). To avoid the uncertainty introduced by non-linear relationship between air pollutant concentration and meteorology, we further estimated the contribution of meteorological and emission variation with *FM* (Eqs. S5-S6). The non-linear effect obtained from various scenarios led to a 0.001-0.08 μg/m^3 difference in the simulated BC concentration induced by meteorological variation, which was minor and of limited influence on the conclusions. We then calculated the average contributions of meteorological and emission variations from *FE* and *FM* during the interval (Eq. S7-S8). Relevant equations are as below:

$$\Delta C_{C_{MET,FE}} = C_{FE,t1} - C_{BASE,t0} \quad \text{(S3)}$$

$$\Delta C_{C_{EMI,FE}} = C_{BASE,t1} - C_{FE,t1} \quad \text{(S4)}$$

$$\Delta C_{C_{MET,FM}} = C_{BASE,t1} - C_{FM,t0} \quad \text{(S5)}$$

$$\Delta C_{C_{EMI,FM}} = C_{FM,t0} - C_{BASE,t0} \quad \text{(S6)}$$

$$\Delta C_{C_{MET}} = \frac{1}{2}(\Delta C_{C_{MET,FE}} + \Delta C_{C_{MET,FM}}) \quad \text{(S7)}$$

$$\Delta C_{C_{EMI}} = \frac{1}{2}(\Delta C_{C_{EMI,FE}} + \Delta C_{C_{EMI,FM}}) \quad \text{(S8)}$$

where *MET* and *EMI* represent two exposure factors (*fe*), i.e., meteorology and emission variation; $\Delta C_{C_{MET,FE}}$ represents changes in BC concentration during the 5-year interval (*t0-t1*) induced by meteorological variation from *FE*; $\Delta C_{C_{EMI,FE}}$ represents changes in BC concentration during the interval induced by emission variation from *FE*; $\Delta C_{C_{MET,FM}}$ represents changes in BC concentration during the interval induced by meteorological variation from *FM*; $\Delta C_{C_{EMI,FM}}$ represents changes in BC concentration during the interval induced by emission variation from *FM*; $C_{FE,t1}$, $C_{FM,t0}$, $C_{BASE,t0}$ and

$C_{BASE,t1}$ represent simulated BC concentrations from *FE*, *FM* and *BASE* for year *t1* and *t0*, respectively; $\Delta C_{C_{MET}}$ represents changes in BC concentration during the 5-year interval (*t0-t1*) induced by meteorological variation; $\Delta C_{C_{EMI}}$ represents changes in BC concentration during the interval (*t0-t1*) induced by emission variation.

Based on a direct proportion approach (Geng et al., 2021), we estimated the contributions of emission and meteorological factors to mortality changes attributed to BC exposure (*ΔME*, Eq. S9-S10). Finally, the total changes in mortality (*ΔM*) can be attributed to five driving factors (Eq. S11):

$$\frac{\Delta C_{fe}}{\Delta C} = \frac{\Delta C_{C_{fe}}}{\sum_{fe=1}^{2} \Delta C_{C_{fe}}}, fe = MET,\ EMI \quad \text{(S9)}$$

$$\Delta ME = \sum_{fe=1}^{2} \Delta M_{fe} = \sum_{fe=1}^{2} \Delta ME \times \frac{\Delta C_{fe}}{\Delta C} \quad \text{(S10)}$$

$$\Delta M = \sum_{fe=1}^{2} \Delta M_{fe} + \sum_{fv=1}^{3} \Delta M_{fv}, fv = P, PS, B \quad \text{(S11)}$$

where ΔC_{fe} represents estimated effect of exposure factor *fe* (i.e., *MET* or *EMI*) on BC concentration change in a given period; *ΔC* represents the simulated BC concentration changes in a given period; *ΔME* represents the total effect of two exposure factors on the change in premature mortality attributable to BC; and *ΔM* represents the total change in premature mortality attributable to BC in a given 5-year interval, which is decomposed into two exposure factors (*fe*, i.e., *MET* or *EMI*) and three vulnerability factors (*fv,* i.e., *P ,PS, B*); *P* is the population, and change in *P* reflects the population change; *PS* is the national proportion of the population subgroup, and change in *PS* reflects the population aging; and *B* is the national baseline mortality rate of all-cause diseases, and change in *B* reflects the improved health care.

Tables

Table S1 Interpretation variables used in XGBoost model and their importance levels in three metrics. Gain is the average gain of splits which use the feature; Cover is the average coverage of splits which use the feature and the coverage is defined as the number of samples affected by the split; and Frequency is the frequency a feature appears in a tree.

ID	Classification	Abbreviation	Full Name	Units	Gain	Cover	Frequency
1	Optical	AAOD MERRA-2	Aerosol Absorption Optical Depth	1	0.225	0.059	0.065
2	Meteorology	PS	Surface pressure	Pa	0.043	0.061	0.053
3	Meteorology	SWGDN	Surface incoming shortwave flux	$W\ m^{-2}$	0.037	0.063	0.056
4	Meteorology	EVAP	Evaporation from turbulence	$kg\ m^{-2}\ s^{-1}$	0.037	0.064	0.057
5	Meteorology	T2M	2-meter max air temperature	K	0.033	0.056	0.054
6	Meteorology	CLDTOT	Total cloud area fraction	1	0.029	0.062	0.060
7	Meteorology	SLP	Sea level pressure	Pa	0.029	0.057	0.059
8	Meteorology	PBLH	Planetary boundary layer height	m	0.026	0.059	0.054
9	Meteorology	U10M	10-meter eastward wind	$m\ s^{-1}$	0.024	0.062	0.058
10	Meteorology	RH	Relative humidity after moist	1	0.024	0.060	0.054
11	Meteorology	V10M	10-meter northward wind	$m\ s^{-1}$	0.022	0.059	0.056
12	Meteorology	PRECTOT	Total precipitation	$kg\ m^{-2}\ s^{-1}$	0.019	0.059	0.055
13	Meteorology	OMEGA	Vertical pressure velocity	$Pa\ s^{-1}$	0.016	0.068	0.055
14	Geography	LON	Longitude	°	0.110	0.025	0.037
15	Geography	LAT	Latitude	°	0.090	0.022	0.033
16	Geography	CROP	Area fraction of crop	1	0.078	0.020	0.023
17	Geography	DEM	Elevation	m	0.027	0.033	0.033

Continued Table S1

ID	Classification	Abbreviation	Full Name	Units	Gain	Cover	Frequency
18	Geography	FOREST	Area fraction of forest	1	0.015	0.025	0.024
19	Geography	GRASS	Area fraction of grass	1	0.011	0.030	0.029
20	Geography	SUBURBAN	Area fraction of suburban	1	0.005	0.015	0.017
21	Geography	WATER	Area fraction of water	1	0.004	0.016	0.017
22	Geography	URBAN	Area fraction of urban	1	0.001	0.008	0.007
23	Temporal	MONTH	Month	1	0.080	0.007	0.015
24	Temporal	YEAR	Year	1	0.017	0.011	0.028

Table S2 Explanation of variables and parameters in equations in this study.

Variables/parameters	Explanation	Appearance
i	the number of grids	Eq. 1, Eq. 2, Eq. 3, Eq. 4, Eq. 5, Eq. 6, Eq. 7, Eq. S1, Eq. S2
j	the number of vertical layers	Eq. 2
m	year	Eq. 1, Eq. 2, Eq. 3, Eq. 4, Eq. 5, Eq. 6, Eq. 7, Eq. S1, Eq. S2
n	month	Eq. 1, Eq. 2, Eq. 3, Eq. 4, Eq. 5, Eq. S1, Eq. S2
MAE	simulated BC MAE	Eq. 1, Eq. 2
$[NA\text{-}PM]$	simulated concentration of total non-absorbing matter (i.e., SO_4^{2-}, NO_3^- and OC)	Eq. 1
$[BC]$	simulated BC concentration	Eq. 1, Eq. 2
$AAOD\_sim$	simulated BC AAOD	Eq. 2, Eq. 4, Eq. 5
z	simulated top of atmosphere	Eq. 2
$z0$	simulated bottom of atmosphere	Eq. 2
dz	height of the vertical layer	Eq. 2
$AAOD\_BC\_xgb$	separated XGBoost BC AAOD	Eq. 3, Eq. 4
$AAOD\_xgb$	XGBoost AAOD	Eq. 3
$AAOD\_BC\_merra2$	MERRA-2 BC AAOD	Eq. 3
$AAOD\_merra2$	MERRA-2 AAOD	Eq. 3
$E_{posterior}$	the posterior BC emissions	Eq. 4
E_{prior}	the prior BC emissions	Eq. 4
α	a unitless factor representing the sensitivity of changes in BC AAOD to changes in BC emissions in each model grid	Eq. 4, Eq. 5
$\Delta E_{perturbed}/E_{prior}$	10% reduction of the prior BC emissions	Eq. 5
$AAOD\_sim_{perturbed}$	simulated BC AAOD with the perturbation	Eq. 5
$\Delta C_{i,m}$	the difference between the posterior simulated average BC concentration of four months in year m of grid i and the health impact thresholds	Eq. 6

Continued Table S2

Variables/parameters	Explanation	Appearance
β_{BC}	the concentration-response coefficient, 0.0204 (95% confidence interval (CI): 0.0187-0.0224)	Eq. 6
AF	attributable fraction of premature mortality to BC exposure	Eq. 6, Eq. 7
P	population	Eq. 7
PS	national proportion of the population subgroup	Eq. 7
B	the national baseline mortality rate of all-cause diseases	Eq. 7
s	population subgroup	Eq. 7
AAE	the absorption Angström exponent obtained from POLDER	Eq. S1, Eq. S2
$AAOD_{POLDER}$	POLDER AAOD at different wavelength	Eq. S1
λ_1	wavelength of 490 nm	Eq. S1, Eq. S2
λ_2	wavelength of 865 nm	Eq. S1, Eq. S2
$AAOD_{OMI}$	OMI AAOD at different wavelength	Eq. S2
MET	exposure factor meteorology	Eq. S3, Eq. S5, Eq. S7
EMI	exposure factor emission	Eq. S4, Eq. S6, Eq. S8
FE	scenarios with fixed emission	Eq. S3, Eq. S4
FM	scenarios with fixed meteorological conditions	Eq. S5, Eq. S6
$t0$	the first year of a five-year interval	Eq. S3, Eq. S5, Eq. S6
$t1$	the last year of a five-year interval	Eq. S3, Eq. S4, Eq. S5
$\Delta C_{C_{MET,FE}}$	changes in BC concentration during the 5-year interval (*t0-t1*) induced by meteorological variation from *FE*	Eq. S3, Eq. S7
$\Delta C_{C_{EMI,FE}}$	changes in BC concentration during the interval induced by emission variation from *FE*	Eq. S4, Eq. S8
$\Delta C_{C_{MET,FM}}$	changes in BC concentration during the interval induced by meteorological variation from *FM*	Eq. S5, Eq. S7

Continued Table S2

Variables/parameters	Explanation	Appearance
$\Delta C_{C_{EMI,FM}}$	changes in BC concentration during the interval induced by emission variation from scenario with *FM*	Eq. S6, Eq. S8
$C_{FE,t1}$	simulated BC concentrations from *FE* for year *t1*	Eq. S3, Eq. S4
$C_{FM,t0}$	simulated BC concentrations from *FM* for year *t0*	Eq. S5, Eq. S6
$C_{BASE,t0}$	simulated BC concentrations from *BASE* for year *t0*	Eq. S3, Eq. S6
$C_{BASE,t1}$	simulated BC concentrations from *BASE* for year *t1*	Eq. S4, Eq. S5
$\Delta C_{C_{MET}}$	changes in BC concentration during the 5-year interval (*t0-t1*) induced by meteorological variation	Eq. S7
$\Delta C_{C_{EMI}}$	changes in BC concentration during the interval (*t0-t1*) induced by emission variation	Eq. S8
ΔC_{fe}	estimated effect of exposure factor *fe* (i.e., *MET* or *EMI*) on BC concentration change in a given period	Eq. S9, Eq. S10
ΔC	the simulated BC concentration changes in a given period	Eq. S9, Eq. S10
fe	two exposure factor, i.e., *MET* or *EMI*	Eq. S9, Eq. S10, Eq. S11
ΔME	the total effect of two exposure factors on the change in premature mortality attributable to BC	Eq. S10
ΔM	the total change in premature mortality attributable to BC in a given 5-year interval	Eq. S11
fv	three vulnerability factors, i.e., *P ,PS, B*	Eq. S11

Table S3 Measured BC concentrations collected from publications (unit: μg/m^3).

Region	Location	Period	Season	BC	References
BTH		1999-2000	annual	9.4	He et al. (2001)
BTH		2001-2002	annual	9.9	Duan et al. (2006)
BTH		1999-2000	spring	6.7	He et al. (2001)
BTH		2001	spring	6.5	Yang et al. (2005a)
BTH		2000	summer	3.1	Song et al. (2006)
BTH		1999-2000	autumn	10.2	He et al. (2001)
BTH		2001	autumn	10.4	Duan et al. (2006)
BTH		2001	autumn	10.7	Yang et al. (2005a)
BTH		1999-2000	winter	11.1	He et al. (2001)
BTH		2001	winter	11.3	Duan et al. (2006)
BTH		2001	winter	9.9	Yang et al. (2005a)
BTH		2005-2006	annual	8.2	Yang et al. (2011)
BTH	Beijing	2005	summer	4.9	Pathak et al. (2011)
BTH		2004	winter	8.3	Song et al. (2007)
BTH		2009-2010	annual	6.3	Zhao et al. (2013)
BTH		2009-2010	annual	5.0	Zhang et al. (2013)
BTH		2009-2010	annual	5.9	Liu et al. (2014)
BTH		2009-2010	annual	5.0	Zhang et al. (2013)
BTH		2009-2010	spring	5.2	Zhao et al. (2013)
BTH		2009-2010	summer	5.9	Zhao et al. (2013)
BTH		2009-2010	summer	4.2	Zhang et al. (2013)
BTH		2009-2010	autumn	7.1	Zhao et al. (2013)
BTH		2009-2010	autumn	5.3	Zhang et al. (2013)
BTH		2009-2010	winter	7.1	Zhao et al. (2013)
BTH		2009-2010	winter	7.5	Zhang et al. (2013)
BTH		2006-2007	winter	8.0	Li et al. (2009)
BTH		2009-2010	annual	6.9	Zhao et al. (2013)
BTH		2008-2009	annual	5.7	Gu et al. (2010)
BTH	Tianjin	2009-2010	spring	5.5	Zhao et al. (2013)
BTH		2009-2010	summer	5.9	Zhao et al. (2013)
BTH		2011	summer	4.9	Wei et al. (2012)
BTH		2009-2010	autumn	8.8	Zhao et al. (2013)
BTH		2009-2010	winter	7.0	Zhao et al. (2013)

Continued Table S3

Region	Location	Period	Season	BC	References
BTH	Chengde	2009-2010	annual	7.3	Zhao et al. (2013)
BTH		2009-2010	spring	4.7	Zhao et al. (2013)
BTH		2009-2010	summer	4.5	Zhao et al. (2013)
BTH		2009-2010	autumn	7.2	Zhao et al. (2013)
BTH		2009-2010	winter	13.1	Zhao et al. (2013)
BTH	Gucheng	2006	annual	12.0	Zhang et al. (2008)
BTH	Shangdianzi	2005	annual	2.5	Zhang et al. (2008)
BTH		2009-2010	annual	3.9	Zhao et al. (2013)
BTH		2009-2010	spring	3.8	Zhao et al. (2013)
BTH		2009-2010	summer	3.3	Zhao et al. (2013)
BTH		2009-2010	autumn	3.9	Zhao et al. (2013)
BTH		2009-2010	winter	4.4	Zhao et al. (2013)
BTH	Shijiazhuang	2009-2010	annual	9.7	Zhao et al. (2013)
BTH		2009-2010	spring	7.8	Zhao et al. (2013)
BTH		2009-2010	summer	7.6	Zhao et al. (2013)
BTH		2009-2010	autumn	11.4	Zhao et al. (2013)
BTH		2009-2010	winter	12.1	Zhao et al. (2013)
YRD	Shanghai	1999-2000	annual	6.5	Ye et al. (2003)
YRD		1999-2000	spring	5.3	Ye et al. (2003)
YRD		1999-2000	summer	5.2	Ye et al. (2003)
YRD		1999-2000	autumn	6.9	Ye et al. (2003)
YRD		1999-2000	winter	8.1	Ye et al. (2003)
YRD		2005-2006	annual	2.9	Feng et al. (2009)
YRD		2005-2006	spring	3.2	Feng et al. (2009)
YRD		2005-2006	summer	2.3	Feng et al. (2009)
YRD		2005-2006	autumn	3.9	Feng et al. (2009)
YRD		2005-2006	winter	2.3	Feng et al. (2009)
YRD		2009	annual	4.1	Zhao et al. (2015b)
YRD		2011-2012	spring	1.7	Zhao et al. (2015a)
YRD		2011-2012	summer	1.4	Zhao et al. (2015a)
YRD		2011-2012	autumn	2.4	Zhao et al. (2015a)
YRD		2011-2012	winter	2.4	Zhao et al. (2015a)
YRD		2015	spring	1.87	Shanghai Academy of Environmental Sciences (Unpublished data from Cheng Huang)
YRD		2015	summer	1.61	
YRD		2015	autumn	1.77	
YRD		2015	winter	2.49	

Continued Table S3

Region	Location	Period	Season	BC	References
YRD		2001	autumn	4.0	Yang et al. (2005b)
YRD		2001	winter	3.1	Yang et al. (2005b)
YRD		2011	spring	3.1	Shen et al. (2014)
YRD		2011	summer	2.6	Shen et al. (2014)
YRD		2011-2014	annual	5.3	Li et al. (2015)
YRD		2011-2014	spring	3.8	Li et al. (2015)
YRD		2011-2014	summer	3.1	Li et al. (2015)
YRD	Nanjing	2011-2014	autumn	5.9	Li et al. (2015)
YRD		2011-2014	winter	8.2	Li et al. (2015)
YRD		2015	spring	1.86	Xiao et al. (2018b)
YRD		2015	summer	2.26	Xiao et al. (2018b)
YRD		2015	autumn	2.54	Xiao et al. (2018b)
YRD		2015	winter	3.47	Xiao et al. (2018b)
YRD		2020	summer	2.98	Tan et al. (2022)
YRD		2020	autumn	1.71	Tan et al. (2022)
YRD		2020	winter	6.98	Tan et al. (2022)
YRD		2015	spring	2.35	Xu et al. (2019)
YRD	Hangzhou-urban	2015	summer	1.12	Xu et al. (2019)
YRD		2015	autumn	2.66	Xu et al. (2019)
YRD		2015	winter	4.68	Xu et al. (2019)
YRD		2015	spring	4.14	Xu et al. (2019)
YRD	Hangzhou-urban	2015	summer	3.41	Xu et al. (2019)
YRD		2015	autumn	3.09	Xu et al. (2019)
YRD		2015	winter	7.89	Xu et al. (2019)
YRD		2015	spring	1.79	Xu et al. (2019)
YRD	Hangzhou-suburban	2015	summer	1.20	Xu et al. (2019)
YRD		2015	autumn	2.01	Xu et al. (2019)
YRD		2015	winter	4.96	Xu et al. (2019)
YRD		2015	spring	2.31	Xu et al. (2019)
YRD	Hangzhou-background	2015	summer	2.13	Xu et al. (2019)
YRD		2015	autumn	2.58	Xu et al. (2019)
YRD		2015	winter	4.30	Xu et al. (2019)
YRD	Changzhou	2015	summer	4.10	Ye et al. (2017)
YRD		2015	autumn	9.62	Ye et al. (2017)
YRD		2015	spring	1.40	Xia et al. (2017)
YRD	Huainan	2015	summer	1.29	Xia et al. (2017)
YRD		2015	autumn	2.40	Xia et al. (2017)
YRD		2015	winter	6.04	Xia et al. (2017)

Continued Table S3

Region	Location	Period	Season	BC	References
YRD	LinAn	2006	annual	4.80	Zhang et al. (2008)
YRD	Ningbo	2009-2010	annual	2.5	Liu et al. (2013)
YRD		2009-2010	spring	3.1	Liu et al. (2013)
YRD		2009-2010	summer	0.8	Liu et al. (2013)
YRD		2009-2010	autumn	1.9	Liu et al. (2013)
YRD		2009-2010	winter	4.1	Liu et al. (2013)
PRD	Guangzhou	2005	spring	10.70	Wu et al. (2013)
PRD		2005	summer	7.60	Wu et al. (2013)
PRD		2005	autumn	8.50	Wu et al. (2013)
PRD		2005	winter	7.50	Wu et al. (2013)
PRD		2009-2010	annual	6.0	Tao et al. (2014c)
PRD		2009	spring	6.1	Tao et al. (2014c)
PRD		2009	summer	3.5	Tao et al. (2014c)
PRD		2009	autumn	6.7	Tao et al. (2014c)
PRD		2010	winter	7.8	Tao et al. (2014c)
PRD		2010	spring	4.60	Wu et al. (2013)
PRD		2010	summer	2.20	Wu et al. (2013)
PRD		2010	autumn	2.90	Wu et al. (2013)
PRD		2010	winter	10.30	Wu et al. (2013)
PRD		2014	annual	4.0	Tao et al. (2017)
PRD		2014	spring	4.2	Tao et al. (2017)
PRD		2014	summer	3.5	Tao et al. (2017)
PRD		2014	autumn	3.6	Tao et al. (2017)
PRD		2014	winter	5.0	Tao et al. (2017)
PRD	Hong Kong	2000-2001	annual	5.4	Louie et al. (2005a)
PRD		2000-2001	spring	5.3	Louie et al. (2005b)
PRD		2000-2001	summer	6.0	Louie et al. (2005b)
PRD		2000-2001	autumn	4.7	Louie et al. (2005b)
PRD		2000-2001	winter	5.0	Louie et al. (2005b)
PRD		2004	summer	3.4	Duan et al. (2007)
PRD		2009-2010	annual	3.6	Yau et al. (2013)
PRD	Shenzhen	2009	annual	4.7	Huang et al. (2014)
PRD		2019-2020	annual	2.79	Chen et al. (2022)
PRD		2019-2020	spring	1.9	Chen et al. (2022)
PRD		2019-2020	summer	2.67	Chen et al. (2022)
PRD		2019-2020	autumn	4.06	Chen et al. (2022)
PRD		2019-2020	winter	2.52	Chen et al. (2022)

Continued Table S3

Region	Location	Period	Season	BC	References
PRD	Panyu	2006	annual	9.30	Zhang et al. (2008)
PRD	Wanqingsha	2009	autumn/winter	5.5	Fu et al. (2014)
SCB	Chengdu	2006	annual	11.10	Zhang et al. (2008)
SCB		2009-2010	annual	9	Tao et al. (2013)
SCB		2009-2010	spring	5.7	Tao et al. (2013)
SCB		2009-2010	summer	7.1	Tao et al. (2013)
SCB		2009-2010	autumn	11.6	Tao et al. (2013)
SCB		2009-2010	winter	11.6	Tao et al. (2013)
SCB		2011	spring	7.0	Tao et al. (2014b)
SCB		2011	autumn	7.0	Tao et al. (2014b)
SCB		2011	summer	6.0	Tao et al. (2014b)
SCB		2011	winter	8.0	Tao et al. (2014b)
SCB	Chongqing	2005-2006	annual	6.4	Yang et al. (2011)
SCB		2019-2020	annual	2.45	Ding et al. (2022)
SCB		2020	winter	5.1	Chen et al. (2020)
Others	Akdala	2005	annual	0.36	Zhang et al. (2008)
Others	Baotou	2011-2012	annual	2.7	Zhang and Zhang (2014)
Others	Changde	2006	annual	2.30	Zhang et al. (2008)
Others	Changsha	2013-2014	spring	4.2	Tang et al. (2017)
Others		2013-2014	summer	2.7	Tang et al. (2017)
Others		2013-2014	autumn	3.9	Tang et al. (2017)
Others		2013-2014	winter	6.0	Tang et al. (2017)
Others	Dalian	2006	annual	5.30	Zhang et al. (2008)
Others	Dunhuang	2006	annual	4.10	Zhang et al. (2008)
Others	Ezhou	2020	winter	2	Wang et al. (2021)
Others	Gaolanshan	2006	annual	3.70	Zhang et al. (2008)
Others	Haikou	2015	annual	1.7	Liu et al. (2017)
Others		2015	spring	1.6	Liu et al. (2017)
Others		2015	summer	0.8	Liu et al. (2017)
Others		2015	autumn	1.8	Liu et al. (2017)
Others		2015	winter	2.4	Liu et al. (2017)
Others	Huanggang	2020	winter	3.7	Wang et al. (2021)
Others	Huangshi	2020	winter	3.8	Wang et al. (2021)
Others	Jinan	2006-2007	annual	4.1	Yang et al. (2012)
Others		2006-2007	spring	3.3	Yang et al. (2012)
Others		2006-2007	summer	3.1	Yang et al. (2012)
Others		2006-2007	autumn	4.5	Yang et al. (2012)

Continued Table S3

Region	Location	Period	Season	BC	References
Others	Jinan	2006-2007	winter	5.7	Yang et al. (2012)
Others		2010	annual	5.3	Gu et al. (2014)
Others	Jinsha	2006	annual	3.2	Zhang et al. (2008)
Others	Lanzhou	2014	annual	9.0	Gu et al. (2014)
Others		2014	spring	6.7	Gu et al. (2014)
Others		2014	summer	4.4	Gu et al. (2014)
Others		2014	autumn	11.5	Gu et al. (2014)
Others		2014	winter	13.4	Gu et al. (2014)
Others		2014	spring	4.7	Gu et al. (2014)
Others		2014	summer	2.8	Gu et al. (2014)
Others		2014	autumn	8.5	Gu et al. (2014)
Others		2014	winter	10.7	Gu et al. (2014)
Others	Lhasa	2006	annual	3.7	Zhang et al. (2008)
Others	Longfengshan	2006	annual	2.4	Zhang et al. (2008)
Others	Nanning	2006	annual	3.7	Zhang et al. (2008)
Others	Qingdao	2020	annual	1.92	Cui et al. (2021b)
Others		2020	spring	1.53	Cui et al. (2021b)
Others		2020	summer	0.83	Cui et al. (2021b)
Others		2020	autumn	1.73	Cui et al. (2021b)
Others		2020	winter	3.65	Cui et al. (2021b)
Others	Qinghai Lake	2010	summer	0.4	Li et al. (2013)
Others	Shangri-La	2005	annual	0.34	Zhang et al. (2008)
Others	Urumqi	2019-2020	summer	2.77	Xu et al. (2021)
Others		2019-2020	autumn	3.74	Xu et al. (2021)
Others		2019-2020	winter	4.72	Xu et al. (2021)
Others	Taiyuan	2019-2020	annual	4.42	Zheng et al. (2022)
Others		2019-2020	spring	5.74	Zheng et al. (2022)
Others		2019-2020	summer	1.07	Zheng et al. (2022)
Others		2019-2020	autumn	11.6	Zheng et al. (2022)
Others		2019-2020	winter	1.22	Zheng et al. (2022)
Others	Waliguan	2020	winter	0.28	Xie et al. (2022)
Others	Wuhan	2011-2012	annual	2.9	Cheng et al. (2012)
Others		2020	winter	2.5	Wang et al. (2021)
Others	Xi'an	2005	annual	13.6	Geng et al. (2017)
Others		2010	annual	8	Wang et al. (2015)

Continued Table S3

Region	Location	Period	Season	BC	References
Others	Xiamen	2009-2010	annual	3.2	Zhang et al. (2011)
Others		2008-2011	annual	1.9	Chen et al. (2012)
Others		2009-2010	spring	2.0	Zhang et al. (2011)
Others		2009-2010	summer	2.3	Zhang et al. (2011)
Others		2009-2010	autumn	3.4	Zhang et al. (2011)
Others		2009-2010	winter	4.9	Zhang et al. (2011)
Others		2009-2010	spring	2.3	Zhang et al. (2012)
Others		2009-2010	summer	2.2	Zhang et al. (2012)
Others		2009-2010	autumn	3.0	Zhang et al. (2012)
Others		2009-2010	winter	4.2	Zhang et al. (2012)
Others	Xianning	2020	winter	3.5	Wang et al. (2021)
Others	Xiaogan	2020	winter	3.1	Wang et al. (2021)
Others	Xinzhou	2020	summer	1.8	Cai et al. (2022)
Others	Yulin	2005	annual	4.00	Zhang et al. (2008)
Others	Yuncheng	2020	autumn	4.5	Li et al. (2022)
Others	Zhengzhou	2006	annual	9.40	Zhang et al. (2008)
Others		2010	annual	3.9	Geng et al. (2013)
Others		2010	spring	3.0	Geng et al. (2013)
Others		2010	summer	1.8	Geng et al. (2013)
Others		2010	autumn	5.4	Geng et al. (2013)
Others		2010	winter	4.7	Geng et al. (2013)
Others		2014-2015	annual	11.0	Wang et al. (2017a)

Table S4 Sensitivity tests designed to quantify the uncertainties to BC emission inversion caused by various factors.

	Wavelength	Description	Uncertainty factors
Base	483 nm	Inversed BC emissions with OMI AAOD at 483 nm. The contributions from BrC and dust AAOD are separated based on MERRA-2 fraction.	-
Test 1	865 nm	Inversed BC emissions with **extrapolated OMI AAOD at 865 nm**, at which the light absorption was seldom influenced by BrC. The contribution from dust AAOD is separated based on MERRA-2 fraction.	Wavelength of AAOD (light-absorption from BrC)
Test 2	865 nm	Inversed BC emissions with extrapolated OMI AAOD at 865 nm, at which the light absorption was seldom influenced by BrC. **The contribution from dust AAOD is separated based on CAMS fraction.**	Light-absorption from dust
Test 3	483 nm	Inversed BC emissions with OMI AAOD at 483 nm. The contributions from BrC and dust AAOD are separated based on MERRA-2 fraction. **The simulated MAE is adjusted based on available measurements.**	Simulated MAE
Test 4	483 nm	Inversed BC emissions with OMI AAOD at 483 nm. The contributions from BrC and dust AAOD are separated based on MERRA-2 fraction. **The simulated BC lifetime in CMAQ model is adjusted to 5.5 days by changing the wet and dry removal rates of BC.**	Simulated BC lifetime

Table S5 MAE measurements collected from publications. Unit: m^2/g.

Region	Site	Year	Season	Wavelength	MAE	Reference
BTH	Tsinghua University	2009	Summer	632	9.41±1.92	Cheng et al. (2011)
BTH	Tsinghua University	2009	Winter	632	8.45±1.71	
BTH	Beijing Mountain	2019	Summer	550	11± 1	Ding et al. (2021)
BTH	Beijing Mountain	2019	Winter	550	10.7 ± 0.9	
BTH	Tiantongyuan community	2014	Annual	632	10.2	Ji et al. (2017)
BTH	IAPCAS	2016	Winter	630	9.5-13.2	Xie et al. (2019)
BTH	Wuqing	2013	Annual	880	6.80±1.13	Xing et al. (2014)
BTH	Wuqing	2013	Spring	880	6.37±1.39	
BTH	Wuqing	2013	Summer	880	8.48±1.25	
BTH	Wuqing	2013	Autumn	880	6.36±1.82	
BTH	Wuqing	2013	Winter	880	5.99±1.08	
BTH	Gucheng	2019	Winter	880	5.5	Zhang et al. (2021)
BTH	NCP	2016	Spring	550	8.21±1.82	Zhao et al. (2019a)
BTH	NCP	2016	Winter	550	8.75±0.18	
YRD	NJU	2015-2017	Summer	678	9.20±0.25	Chen et al. (2019a)
YRD	NJU	2015-2017	Autumn	678	8.47±0.57	
YRD	NJU	2015-2017	Winter	678	8.70±0.48	
YRD	NUIST	2015-2017	Summer	678	11.10±0.68	
YRD	NUIST	2015-2017	Autumn	678	10.20±0.77	
YRD	NUIST	2015-2017	Winter	678	10.50±0.98	

Continued Table S5

Region	Site	Year	Season	Wavelength	MAE	Reference
YRD	PAES	2015-2017	Summer	678	8.81±0.77	Chen et al. (2019a)
YRD	PAES	2015-2017	Autumn	678	8.42±0.76	
YRD	PAES	2015-2017	Winter	678	8.31±0.53	
YRD	NUIST	2013	Spring	781	11.2±2.9	Cui et al. (2021a)
YRD	NUIST	2012-2013	Summer	781	9.9±1.9	
YRD	NUIST	2012	Autumn	781	7.2±1.9	
YRD	NUIST	2013	Winter	781	12.5±3.1	
YRD	Haining	2013	Annual	880	8.11±1.87	Xing et al. (2014)
YRD	Haining	2013	Spring	880	7.32	
YRD	Haining	2013	Summer	880	9.67±0.70	
YRD	Haining	2013	Autumn	880	5.82±0.47	
YRD	Haining	2013	Winter	880	9.6±3.6	
PRD	PKU-SZ	2011	Summer	532	6.5±0.5	Lan et al. (2013)
PRD	SZ	2015	Summer	405	11.8	Li et al. (2018)
PRD	SZ	2015	Autumn	405	13.4	
PRD	JNU	2017	Summer	520	10.73±4.96	Sun et al. (2020)
PRD	JNU	2017-2018	Winter	520	18.47±5.49	
PRD	SCIES	2015-2016	Annual	550	9.3	Tao et al. (2021)
PRD	SCIES	2015-2016	Spring	550	10.1±1.0	
PRD	SCIES	2015-2016	Summer	550	8.9±0.7	

Continued Table S5

Region	Site	Year	Season	Wavelength	MAE	Reference
PRD	SCIES	2015-2016	Autumn	550	9.1±1.0	Tao et al. (2021)
PRD	SCIES	2015-2016	Winter	550	9.1±0.7	
PRD	NC	2012-2013	Annual	550	18.75±6.16	Wu et al. (2018a)
PRD	NC	2012-2013	Spring	550	19.91	
PRD	NC	2012-2013	Summer	550	22.18	
PRD	NC	2012-2013	Autumn	550	16.81	
PRD	NC	2012-2013	Winter	550	17.38	
PRD	Zhongshan	2013	Annual	880	7.77±1.51	Xing et al. (2014)
PRD	Zhongshan	2013	Spring	880	6.97	
PRD	Zhongshan	2013	Summer	880	8.75	
PRD	Zhongshan	2013	Autumn	880	9.22±1.27	
PRD	Zhongshan	2013	Winter	880	5.94	
SCB	CRAES	2011	Spring	520	15.6±0.2	Tao et al. (2014a)
SCB	CRAES	2011	Summer	520	14.4±0.2	
SCB	CRAES	2011	Autumn	520	14.3±0.3	
SCB	CRAES	2011	Winter	520	10.5±0.1	
SCB	Deyang	2013	Annual	880	7.37±1.93	Xing et al. (2014)
SCB	Deyang	2013	Spring	880	5.18±0.38	
SCB	Deyang	2013	Summer	880	8.39	
SCB	Deyang	2013	Autumn	880	9.46±1.61	
SCB	Deyang	2013	Winter	880	6.43	

Continued Table S5

Region	Site	Year	Season	Wavelength	MAE	Reference
Others	Mt. Tai	2014	Summer	678	7.8±2.7	Bai et al. (2018)
Others	SDUMS	2014	Summer	678	7.4±2.6	
Others	Qingdao	2018	Summer	678	7.12±1.82	Cao et al. (2021)
Others	Qingdao	2018	Autumn	678	6.66±1.56	
Others	SDUMS	2014	Winter	678	9.0±2.3	Chen et al. (2017a)
Others	Beiluhe	2015-2016	Annual	632	11.8±6.60	Chen et al. (2019b)
Others	Everest	2014-2016	Annual	632	8.18±2.83	
Others	Lanzhou	2015-2016	Annual	632	7.07±4.08	
Others	Laohugou	2015-2016	Annual	632	8.09±2.86	
Others	Lhasa	2013-2015	Annual	632	7.58±2.25	
Others	Lulang	2014-2015	Annual	632	8.65±1.55	
Others	Ngari	2015-2016	Annual	632	14.3±6.54	
Others	Nyalam	2013-2015	Annual	632	8.61±3.36	
Others	Yulong	2015-2016	Annual	632	7.43±3.03	
Others	Zhongba	2013-2015	Annual	632	8.04±2.79	
Others	Yucheng	2014	Summer	678	9.58±1.83	Cui et al. (2016)
Others	Lhasa	2013-2014	Summer	632	8.10±0.98	Hu et al. (2017)
Others	Nam Co	2014	Summer	632	6.10±1.21	
Others	Ganhaizi	2014-2016	Annual	632	6.25±0.46	Niu et al. (2018)
Others	Ganhaizi	2014-2016	Spring	632	5.68	

Continued Table S5

Region	Site	Year	Season	Wavelength	MAE	Reference
Others	Ganhaizi	2014-2016	Summer	632	9.95	Niu et al. (2018)
Others	Ganhaizi	2014-2016	Autumn	632	5.83	
Others	Ganhaizi	2014-2016	Winter	632	3.53	
Others	Yulong	2014-2016	Annual	632	7.38±1.01	
Others	Yulong	2014-2016	Spring	632	10.48	
Others	Yulong	2014-2016	Summer	632	7.10	
Others	Yulong	2014-2016	Autumn	632	3.78	
Others	Yulong	2014-2016	Winter	632	5.36	
Others	IEECAS	2013	Winter	532	14.6±5.6	Wang et al. (2017b)
Others	Zhangye	2014	Spring	550	9.8	Wu et al. (2018b)
Others	Xian	2014	Summer	880	10.1	Zhang et al. (2019)
Others	Xian	2014	Winter	880	6.55	
Others	Lanzhou	2015-2016	Summer	632	6.9	Zhang and Kang (2019)
Others	Lanzhou	2015-2016	Winter	632	7.5	
Others	Lulang	2008-2009	Annual	405	6.07	Zhao et al. (2019b)
Others	Lulang	2008-2009	Spring	405	6.36	
Others	Lulang	2008-2009	Summer	405	6.56	
Others	Lulang	2008-2009	Autumn	405	6.17	
Others	Lulang	2008-2009	Winter	405	4.92	

Table S6 Comparison between the posterior simulated and measured MAE. OBS is mean measured MAE (at the wavelength of 483nm, m^2/g), SIM is mean simulated MAE, BIAS is mean bias between SIM and OBS.

Comparison by Region						
	OBS (m^2/g)	SIM (m^2/g)	BIAS (m^2/g)	NMB	NME	RMSE (m^2/g)
BTH	12.21	10.14	-2.07	-16.97%	18.06%	2.62
YRD	13.67	10.23	-3.43	-15.17%	25.34%	3.11
PRD	13.43	10.26	-3.17	-19.59%	24.16%	3.74
SCB	14.01	10.30	-3.71	-21.55%	28.32%	4.64
Others	11.47	10.13	-1.34	-10.97%	17.69%	2.89

Comparison by Season						
	OBS (m^2/g)	SIM (m^2/g)	BIAS (m^2/g)	NMB	NME	RMSE (m^2/g)
Annual	12.05	10.23	-1.83	-15.16%	19.63%	3.38
Spring	11.85	9.94	-1.92	-16.16%	21.57%	3.10
Summer	12.43	10.05	-2.38	-19.17%	23.58%	3.76
Autumn	12.91	10.48	-2.43	-18.80%	23.03%	3.93
Winter	12.71	10.23	-2.48	-19.54%	22.21%	4.03

Table S7 Scenarios designed to quantify drivers (i.e., meteorology and emissions) of changes in premature mortality attributable to BC exposure.

	Simulation year	Year of the posterior emissions in China	Year of meteorological conditions
BASE	2000	2000	2000
	2005	2005	2005
	2010	2010	2010
	2015	2015	2015
	2020	2020	2020
Fix emission (*FE*)	2005	2000	2005
	2010	2005	2010
	2015	2010	2015
	2020	2015	2020
Fix meteorology (*FM*)	2000	2005	2000
	2005	2010	2005
	2010	2015	2010
	2015	2020	2015

Table S8 Evaluation of the monthly XGBoost fitting in 10-fold cross validation and ground measurement validation.

	10-fold Cross-Validation with OMI				Ground Measurement Validation			
Year	Sample size	RMSE	NMB	NME	Sample size	RMSE	NMB	NME
2001	-	-	-	-	13	0.0249	-7.79%	27.53%
2002	-	-	-	-	14	0.0172	-11.93%	23.55%
2003	-	-	-	-	11	0.0177	-8.36%	22.48%
2004	-	-	-	-	15	0.0208	-10.75%	30.68%
2005	51000	0.0141	-3.57%	19.60%	25	0.0155	-3.33%	21.08%
2006	51944	0.0140	-3.42%	19.10%	44	0.0204	10.83%	32.98%
2007	56794	0.0132	-3.50%	19.63%	55	0.0194	7.92%	36.54%
2008	54778	0.0135	-3.54%	19.56%	97	0.0183	-1.46%	30.28%
2009	47993	0.0138	-4.52%	21.25%	58	0.0190	5.42%	33.08%
2010	40893	0.0129	-4.18%	20.43%	68	0.0165	5.29%	32.48%
2011	41927	0.0131	-4.08%	20.53%	65	0.0170	1.32%	31.29%
2012	41830	0.0147	-4.21%	20.78%	70	0.0131	8.19%	28.43%
2013	44823	0.0132	-3.92%	20.33%	58	0.0216	14.99%	36.43%
2014	45600	0.0119	-3.64%	20.01%	52	0.0182	6.81%	30.87%
2015	36035	0.0132	-4.35%	21.29%	276	0.0173	3.28%	34.97%
2016	31593	0.0130	-4.41%	21.34%	177	0.0177	4.58%	32.60%
2017	28580	0.0128	-4.70%	22.23%	169	0.0145	0.54%	29.42%
2018	16004	0.0119	-4.62%	21.64%	244	0.0163	1.49%	32.26%

Continued Table S8

	10-fold Cross-Validation with OMI				Ground Measurements Validation			
Year	Sample size	RMSE	NMB	NME	Sample size	RMSE	NMB	NME
2019	7730	0.0140	-4.45%	22.52%	222	0.0179	3.88%	32.05%
2020	4564	0.0149	-4.72%	22.28%	28	0.0106	1.37%	31.53%

Note: The NMB, NME and RMSE were calculated using following equations (P and O indicate the results from XGBoost prediction and observation, respectively):

$$NMB = \frac{\sum_{i=1}^{n}(P_i - O_i)}{\sum_{i=1}^{n} O_i} \times 100\%;\ NME = \frac{\sum_{i=1}^{n}|P_i - O_i|}{\sum_{i=1}^{n} O_i};\ RMSE = \sqrt{\frac{1}{n}\sum_{i=1}^{n}(P_i - O_i)^2}$$

Table S9 Evaluation of the monthly XGBoost performance against OMI and ground measurements for different OMI coverage levels.

	OMI Coverage	BIAS	RMSE	NMB	NME
OMI	<20%	-0.0024	0.0165	-4.99%	21.28%
	20%-60%	-0.0015	0.0130	-3.68%	19.98%
	>60%	-0.0010	0.0101	-3.37%	20.58%
Ground measurement	<20%	0.0035	0.0186	8.75%	35.86%
	20%-60%	0.0022	0.0178	4.73%	29.99%
	>60%	0.0011	0.0149	3.08%	31.43%

Table S10 Meteorology performance in 2000-2020 (with a five-year interval). OBS is mean observations, PRE is mean predictions, BIAS is mean bias, NMB is normalized mean bias, NME is normalized mean error, IOA is index of agreement. The benchmarks for temperature (BIAS within ± 0.5 K), wind speed (BIAS within ± 0.5 m/s) and wind direction (BIAS within ± 10°) are suggested by Emery et al. (2001).

Parameter	Year	OBS	PRE	BIAS	NMB	NME	IOA
Temperature (°C)	2000	11.9	10.8	-1.1	-9.0%	28.5%	0.97
	2005	12.7	11.6	-1.1	-8.3%	25.8%	0.97
	2010	12.2	11.9	-0.3	-2.1%	24.8%	0.98
	2015	12.8	12.4	-0.3	-2.5%	24.2%	0.98
	2020	12.7	12.1	-0.6	-4.7%	20.2%	0.98
Relative humidity (%)	2000	69.2	66.0	-3.2	-4.7%	19.6%	0.81
	2005	65.2	63.4	-1.8	-5.7%	20.3%	0.81
	2010	68.7	66.2	-2.6	-3.8%	20.9%	0.84
	2015	71.0	63.0	-8.0	-11.2%	26.3%	0.85
	2020	67.6	62.4	-5.3	-7.8%	20.1%	0.86
Wind speed (m/s)	2000	2.5	3.5	1.0	31.9%	68.9%	0.64
	2005	2.5	3.2	0.7	34.9%	77.6%	0.63
	2010	2.5	3.0	0.5	32.5%	72.7%	0.66
	2015	2.6	3.4	0.8	30.3%	73.6%	0.66
	2020	2.5	3.0	0.5	30.9%	66.3%	0.69
Wind direction (°)	2000	147.2	173.6	26.4	17.9%	76.3%	0.57
	2005	171.4	179.6	8.2	4.8%	58.1%	0.59
	2010	168.5	164.1	-4.4	-2.6%	58.4%	0.61
	2015	177.9	163.9	-14.0	-7.9%	56.3%	0.60
	2020	176.1	172.5	-3.6	-2.0%	48.9%	0.65

Table S11 Comparison between XGBoost predictions and simulations for 2000-2020 (with a five-year interval). BIAS is mean bias between simulated and XGBoost predicted BC AAOD.

		The prior simulation					The posterior simulation				
Year	Month	BIAS	R	NMB	NME	RMSE	BIAS	R	NMB	NME	RMSE
2000	1	-0.024	0.57	-47.19%	48.05%	0.032	0.007	0.79	13.8%	27.3%	0.019
2000	4	-0.034	0.76	-75.11%	75.19%	0.038	-0.001	0.88	-1.86%	15.61%	0.01
2000	7	-0.041	0.15	-82.11%	82.17%	0.049	-0.003	0.73	-6.87%	27.68%	0.019
2000	10	-0.028	0.69	-73.55%	73.62%	0.032	0.000	0.91	-0.46%	16.97%	0.008
2005	1	-0.032	0.53	-47.9%	49.53%	0.045	0.008	0.75	12.3%	25.71%	0.026
2005	4	-0.046	0.76	-75.68%	75.79%	0.05	0.000	0.9	-0.05%	14.66%	0.012
2005	7	-0.044	0.16	-80.23%	80.31%	0.052	-0.003	0.74	-4.85%	25.99%	0.019
2005	10	-0.028	0.76	-59.72%	60.34%	0.035	0.003	0.92	6.3%	18.07%	0.011
2010	1	-0.016	0.77	-31.91%	35.37%	0.023	0.004	0.89	8.25%	18.18%	0.013
2010	4	-0.039	0.74	-77.26%	77.31%	0.043	-0.002	0.85	-3.83%	17.54%	0.012
2010	7	-0.039	0.22	-75.36%	75.6%	0.046	0.001	0.73	2.44%	27.7%	0.018
2010	10	-0.026	0.84	-58.95%	59.35%	0.033	0.003	0.95	6.85%	16.34%	0.01
2015	1	-0.014	0.81	-29.22%	33.83%	0.02	0.006	0.91	12.73%	18.93%	0.012
2015	4	-0.04	0.84	-77.07%	77.13%	0.044	-0.001	0.91	-1.65%	14.51%	0.01
2015	7	-0.032	0.55	-69.8%	69.89%	0.036	-0.001	0.86	-3.2%	17.52%	0.011
2015	10	-0.021	0.86	-53.58%	54.27%	0.028	0.003	0.95	8.51%	16.78%	0.009

Continued Table S11

		The prior simulation					The posterior simulation				
Year	Month	BIAS	R	NMB	NME	RMSE	BIAS	R	NMB	NME	RMSE
2020	1	-0.038	0.59	-59.56%	59.8%	0.048	0.007	0.88	10.5%	22.44%	0.019
2020	4	-0.036	0.7	-74.71%	74.81%	0.04	0.000	0.79	-0.29%	18.31%	0.013
2020	7	-0.038	0.24	-85.03%	85.07%	0.044	-0.005	0.75	-10.7%	28.22%	0.017
2020	10	-0.03	0.82	-74.12%	74.19%	0.038	0.001	0.94	2.9%	17.78%	0.01

Note: The BIAS, NMB, NME and RMSE were calculated using following equations (P and O indicate the results from model simulation and XGBoost prediction, respectively):

$$BIAS = \frac{1}{n}\sum_{i=1}^{n}(P_i - O_i);\ NMB = \frac{\sum_{i=1}^{n}(P_i - O_i)}{\sum_{i=1}^{n} O_i} \times 100\%;\ NME = \frac{\sum_{i=1}^{n}|P_i - O_i|}{\sum_{i=1}^{n} O_i};\ RMSE = \sqrt{\frac{1}{n}\sum_{i=1}^{n}(P_i - O_i)^2}$$

Table S12 Total premature mortality associated with BC exposure and drivers of changing premature mortality by province during 2000-2020 with five-year interval (Unit: thousand cases). The red and blue present the increase and reduction of premature mortality associated to changing drivers, and darker colors indicate greater changes in premature mortality.

	2000	P	PS	B	EMI	MET	2005	P	PS	B	EMI	MET	2010	P	PS	B	EMI	MET	2015	P	PS	B	EMI	MET	2020
Anhui	30.6	-0.1	4.6	-3.2	8.5	4.5	44.8	-0.4	7.0	-6.2	10.1	-8.0	47.3	-0.3	7.7	-6.6	-1.9	1.5	47.8	-0.9	5.8	-2.7	-8.5	3.8	45.0
Beijing	6.6	1.5	1.1	-0.7	2.1	0.5	11.0	2.0	1.8	-1.6	0.1	-0.8	12.5	2.3	2.2	-1.9	-0.2	0.0	14.9	2.4	2.1	-1.0	0.2	-0.4	18.5
Chongqing	19.9	-0.7	2.6	-1.8	0.6	1.8	22.4	-0.9	3.2	-2.8	-1.6	-0.7	19.6	-0.7	2.9	-2.5	-5.5	2.2	16.1	-1.0	2.4	-1.1	-0.3	2.8	18.8
Fujian	9.8	0.3	1.2	-0.9	0.0	0.1	10.5	0.2	1.7	-1.5	-3.8	4.8	11.9	0.3	1.8	-1.5	-5.3	2.3	9.6	0.2	1.3	-0.6	0.7	-1.0	10.1
Gansu	9.6	0.1	1.4	-1.0	2.0	0.6	12.7	0.0	1.6	-1.4	-4.0	-0.7	8.2	0.0	1.3	-1.1	-1.7	0.5	7.2	-0.1	1.1	-0.5	0.4	1.5	9.5
Guangdong	26.8	2.6	3.6	-2.5	-4.5	5.9	31.8	2.8	5.3	-4.7	14.5	-11.4	38.4	2.9	5.6	-4.7	-21.5	9.1	29.8	2.3	4.3	-2.0	0.3	0.0	34.6
Guangxi	16.6	0.4	2.4	-1.7	0.5	4.5	22.8	0.3	3.5	-3.1	0.1	-0.1	23.4	0.3	3.3	-2.8	-11.3	4.1	17.1	0.0	2.4	-1.1	0.4	0.4	19.2
Guizhou	19.3	-0.2	2.6	-1.8	0.4	2.2	22.5	-0.3	3.2	-2.8	-0.4	-2.6	19.6	-0.2	3.3	-2.8	-6.1	7.3	21.1	-0.5	3.0	-1.4	1.3	-0.2	23.3
Hainan	1.7	0.1	0.2	-0.2	-0.1	0.4	2.2	0.1	0.3	-0.3	0.0	0.0	2.4	0.1	0.3	-0.3	-1.6	0.7	1.6	0.1	0.3	-0.1	0.6	-0.3	2.2
Hebei	36.7	1.4	5.1	-3.6	6.2	1.4	47.2	1.2	7.0	-6.2	-7.3	2.9	44.9	1.2	7.5	-6.3	-0.2	0.0	47.0	0.7	7.0	-3.3	0.0	5.8	57.2
Heilongjiang	42.5	1.4	5.2	-3.7	1.6	-4.4	42.7	1.2	7.0	-6.2	3.8	2.0	50.4	1.4	8.6	-7.3	-0.8	2.8	55.1	0.7	7.3	-3.4	-11.6	4.9	53.1
Henan	61.9	0.9	8.5	-6.0	7.1	5.1	77.6	0.3	11.0	-9.7	-13.6	1.9	67.5	0.4	10.8	-9.1	-5.8	1.1	64.8	-0.3	10.3	-4.8	7.2	11.8	88.9
Hubei	31.5	-0.7	4.7	-3.3	8.8	4.6	45.6	-1.0	6.9	-6.1	-0.8	0.1	44.7	-0.8	6.5	-5.5	-11.7	1.8	35.1	-1.2	4.9	-2.3	-0.1	1.9	38.2
Hunan	34.7	0.6	5.0	-3.5	6.4	4.9	48.1	0.3	7.0	-6.2	-3.2	-2.1	43.8	0.3	6.5	-5.5	-9.4	0.6	36.2	-0.2	5.5	-2.6	0.1	6.8	45.9
Inner Mongolia	7.4	0.2	1.0	-0.7	1.4	0.1	9.4	0.1	1.3	-1.1	-1.7	-0.6	7.4	0.1	1.1	-1.0	-2.0	0.9	6.5	0.0	1.0	-0.5	-4.2	5.5	8.3
Jiangsu	34.4	0.9	5.0	-3.5	7.4	4.3	48.4	1.0	8.0	-7.1	14.6	-7.1	57.8	1.5	10.1	-8.6	0.7	5.8	67.3	0.8	8.2	-3.8	-20.5	1.8	53.9
Jiangxi	14.9	0.8	2.2	-1.5	0.5	4.2	21.0	0.8	3.2	-2.8	4.7	-5.6	21.3	0.8	3.2	-2.7	-6.0	1.4	17.9	0.5	2.7	-1.3	0.1	2.5	22.5
Jilin	40.0	0.4	4.8	-3.4	-0.7	-2.6	38.5	0.1	5.9	-5.3	7.6	-7.1	39.9	0.2	6.6	-5.6	-1.0	0.9	41.0	-0.4	5.2	-2.4	-9.8	2.8	36.4
Liaoning	52.2	1.0	5.8	-4.1	-3.5	-8.9	42.5	0.5	6.3	-5.6	10.6	-13.5	40.9	0.5	6.2	-5.3	-13.1	6.1	35.4	0.0	4.7	-2.2	-7.0	3.2	34.0
Ningxia	1.6	0.1	0.2	-0.2	0.5	0.0	2.4	0.1	0.3	-0.3	-0.9	0.0	1.6	0.1	0.3	-0.2	-0.2	0.1	1.7	0.1	0.3	-0.1	0.2	0.2	2.3
Qinghai	1.5	0.1	0.2	-0.1	0.2	0.0	1.8	0.1	0.2	-0.2	-0.5	-0.2	1.2	0.1	0.2	-0.2	-0.3	0.1	1.1	0.1	0.2	-0.1	-0.5	0.9	1.7
Shandong	46.2	1.3	6.9	-4.8	13.5	3.8	66.9	1.1	10.4	-9.2	1.0	0.2	70.3	1.2	11.9	-10.1	-2.6	5.5	76.3	0.2	10.7	-5.0	-1.8	1.4	81.8

Continued Table S12

	2000	P	PS	B	EMI	MET	2005	P	PS	B	EMI	MET	2010	P	PS	B	EMI	MET	2015	P	PS	B	EMI	MET	2020
Shanghai	9.2	1.6	1.2	-0.9	0.8	-0.9	11.0	2.0	1.9	-1.7	9.9	-8.6	14.5	2.5	2.6	-2.2	-0.2	0.6	17.8	2.2	2.1	-1.0	-10.7	1.9	12.3
Shaanxi	19.9	0.5	2.7	-1.9	2.5	1.1	24.8	0.3	3.4	-3.0	-5.9	0.0	19.5	0.3	2.9	-2.5	-5.9	2.1	16.5	0.0	2.7	-1.3	2.4	3.5	23.8
Shanxi	29.6	1.4	3.8	-2.7	0.6	0.0	32.7	1.0	4.1	-3.6	-14.3	0.6	20.5	0.8	3.3	-2.8	-2.3	0.4	19.9	0.6	3.5	-1.7	6.2	4.7	33.3
Sichuan	59.2	-1.3	7.9	-5.6	7.5	3.0	70.7	-1.6	10.1	-8.9	-8.4	0.3	62.2	-0.9	9.2	-7.7	-19.3	6.7	50.1	-1.3	7.0	-3.3	-1.3	2.6	53.9
Tianjin	5.5	0.8	0.8	-0.6	0.7	0.2	7.4	1.0	1.3	-1.1	0.2	0.6	9.4	1.2	1.7	-1.4	-0.2	0.5	11.2	1.3	1.7	-0.8	1.2	-1.1	13.6
Xinjiang	1.2	0.1	0.2	-0.1	0.3	0.2	1.9	0.1	0.3	-0.2	0.0	-0.5	1.6	0.1	0.3	-0.2	-0.4	0.2	1.6	0.1	0.3	-0.1	0.3	0.3	2.5
Tibet	0.1	0.0	0.0	0.0	0.0	0.0	0.1	0.0	0.0	0.0	0.0	0.0	0.1	0.0	0.0	0.0	0.0	0.0	0.1	0.0	0.0	0.0	0.0	0.0	0.1
Yunnan	16.2	0.7	2.2	-1.5	0.9	1.5	19.9	0.6	2.9	-2.6	0.5	-2.4	18.9	0.6	3.1	-2.6	-1.9	1.3	19.4	0.3	2.8	-1.3	3.4	-1.7	22.9
Zhejiang	14.4	1.3	2.0	-1.4	0.2	2.1	18.5	1.5	3.0	-2.7	-11.4	12.7	21.6	1.8	3.7	-3.1	-10.8	11.0	24.1	1.5	3.2	-1.5	-10.0	5.7	23.0

Table S13 The concentration-response coefficients and corresponding all-cause premature deaths attributed to BC exposure estimated in this study for China.

β_{BC} (95% CI)	Reference	Description	Premature mortality in thousand (95% CI)
0.020 (0.019-0.022)	Chen et al. (2021)	A prospective cohort in Deqing of Zhejiang, China.	734~938 (677, 1023)
0.058 (0.049-0.068)	Janssen et al. (2011)	A meta-analysis of time-series studies conducted in the United States and European countries.	1851~2386 (1596, 2700)
0.006 (0.005-0.007)	Krewski et al. (2009)	A prospective cohort study that includes a large population (500,000 adults) over 116 cities in the United States.	221~281 (185, 326)

Figures

Figure S1 Definition of (a) provinces, key regions and observation sites and (b) land-use types of study domain. (a) The large rectangle presents the simulation domain of CMAQ model. The small rectangle presents the Eastern China. Regions apart from the Eastern China were defined as the rest of China. Chinese mainland, Hong Kong, Macao and Taiwan are study domain of XGBoost model. The blue circles present the locations of AAOD monitoring sites (including 116 sites from four aerosol monitoring networks), the green triangles present the locations of BC concentration monitoring sites collected from literatures (Supplementary Table S5), the red rectangles present the locations of MAE measured sites collected from literatures (Supplementary Table S6). Key regions are presented by different blue filling. BTH represents Beijing-Tianjin-Hebei, YRD represents Yangtze River Delta, PRD represents Pearl River Delta, FWP represents Fenwei Plain, SCB represents Sichuan Basin and NE represents Northeastern China. (b) Spatial distribution of different land-use types of China.

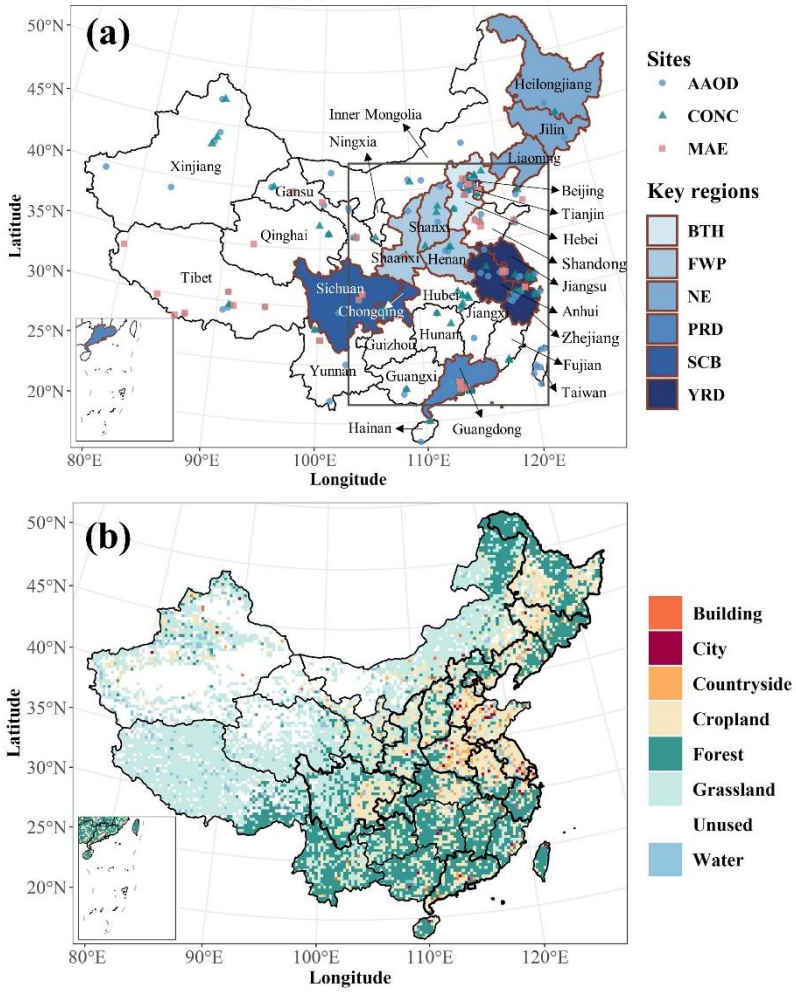

Figure S2 Spatial distribution of multiyear annual average OMI AAOD coverage.

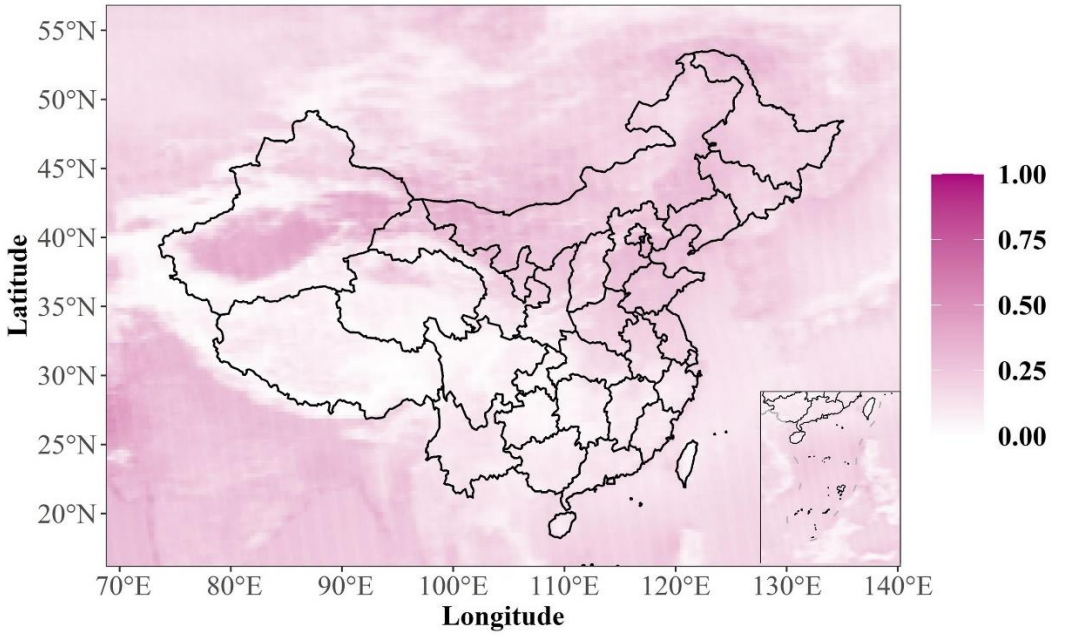

Figure S3 Multiyear average fractions of dust AAOD to AAOD from MERRA-2 (a) and CAMS (b).

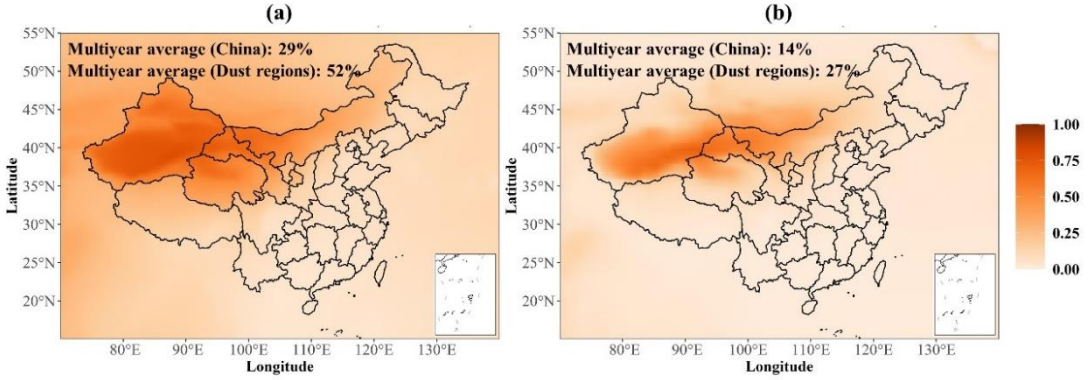

Figure S4 WRF-CMAQ simulated daily BC lifetimes for different months in base case and Test 4. The boxes represent the 25th to 75th percentiles of the distributions while the solid lines within each box represent the means.

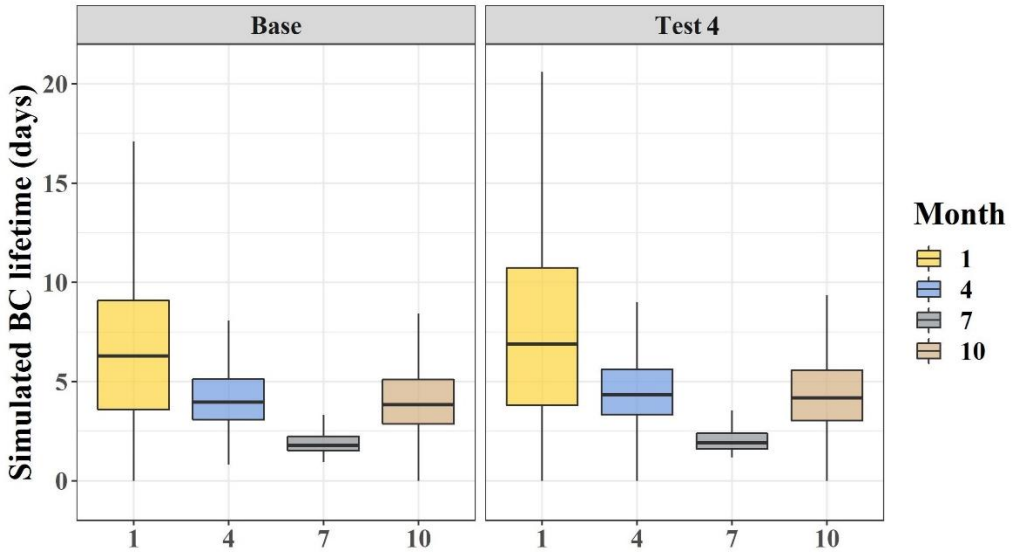

Figure S5 Comparison between XGBoost prediction and ground observation AAOD for regional representative sites in 2000-2020. N represents number of monthly observation data.

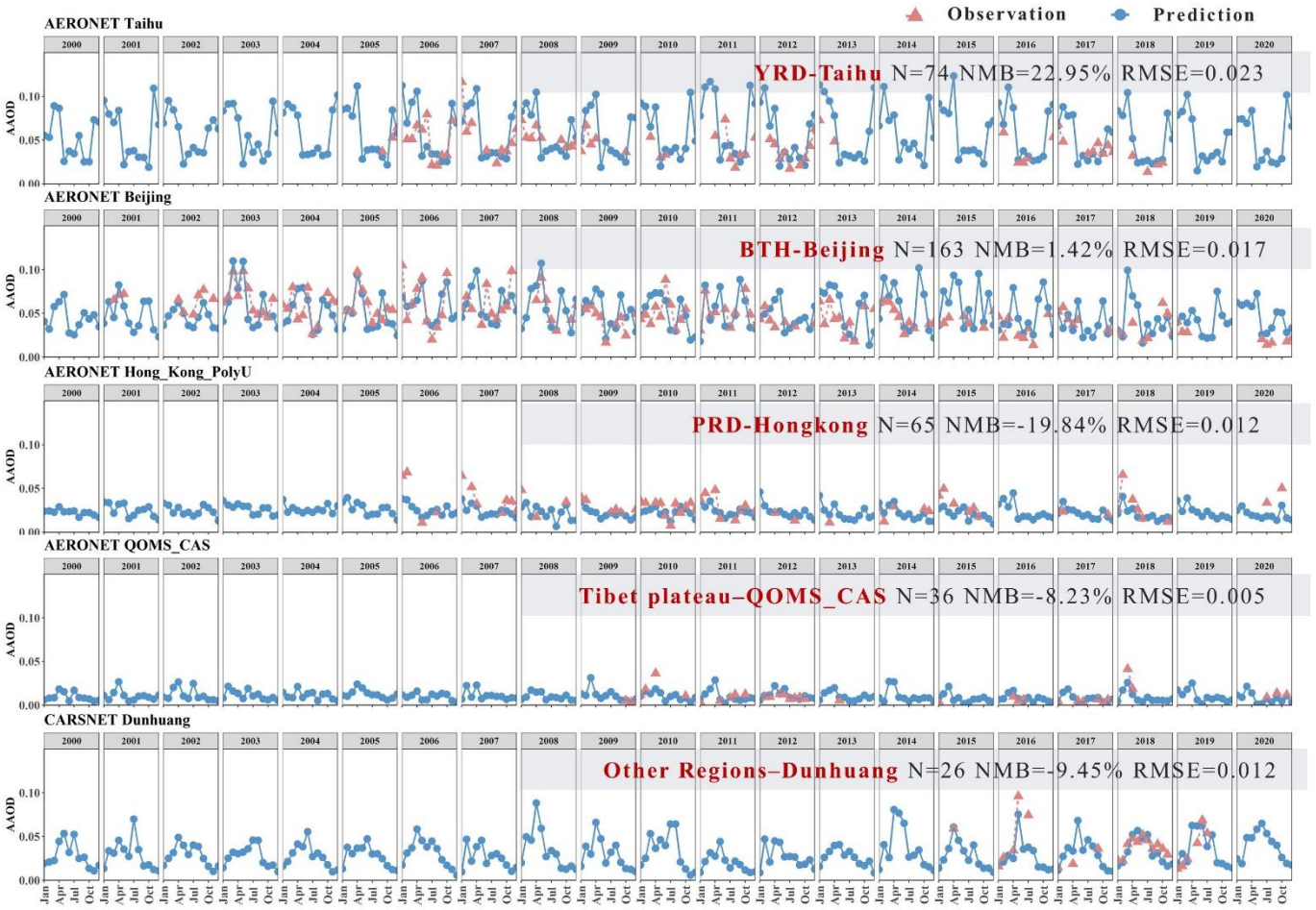

Figure S6 Evaluation of the prior (blued dots) and posterior (red dots) simulated monthly surface BC concentration in China by year with observations collected from publications (from 2000-2020, with a five-year-interval). The BIAS, NMB, NME, slope of the linear fitting (SLOPE) and number of samples (NUM.) are provided in the top left corner.

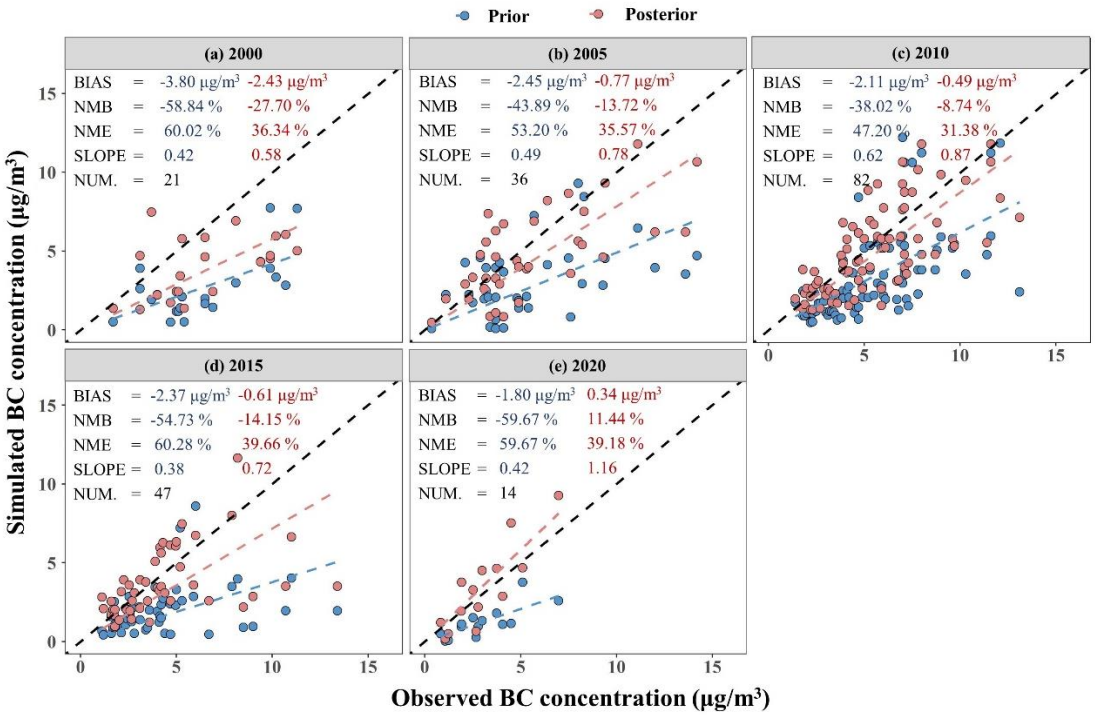

Note: The BIAS, NMB and NME were calculated using following equations (P and O indicate the results from model simulation and observation, respectively):

$$BIAS = \frac{1}{n}\sum_{i=1}^{n}(P_i - O_i)$$

$$NMB = \frac{\sum_{i=1}^{n}(P_i - O_i)}{\sum_{i=1}^{n} O_i} \times 100\%$$

$$NME = \frac{\sum_{i=1}^{n}|P_i - O_i|}{\sum_{i=1}^{n} O_i}$$

Figure S7 Evaluation of the prior (blued dots) and posterior (red dots) simulated monthly surface BC concentration of different land-use types in China with observations collected from publications (from 2000-2020, with a five-year-interval). The BIAS, NMB, NME, slope of the linear fitting (SLOPE) and number of samples (NUM.) are provided in the top left corner.

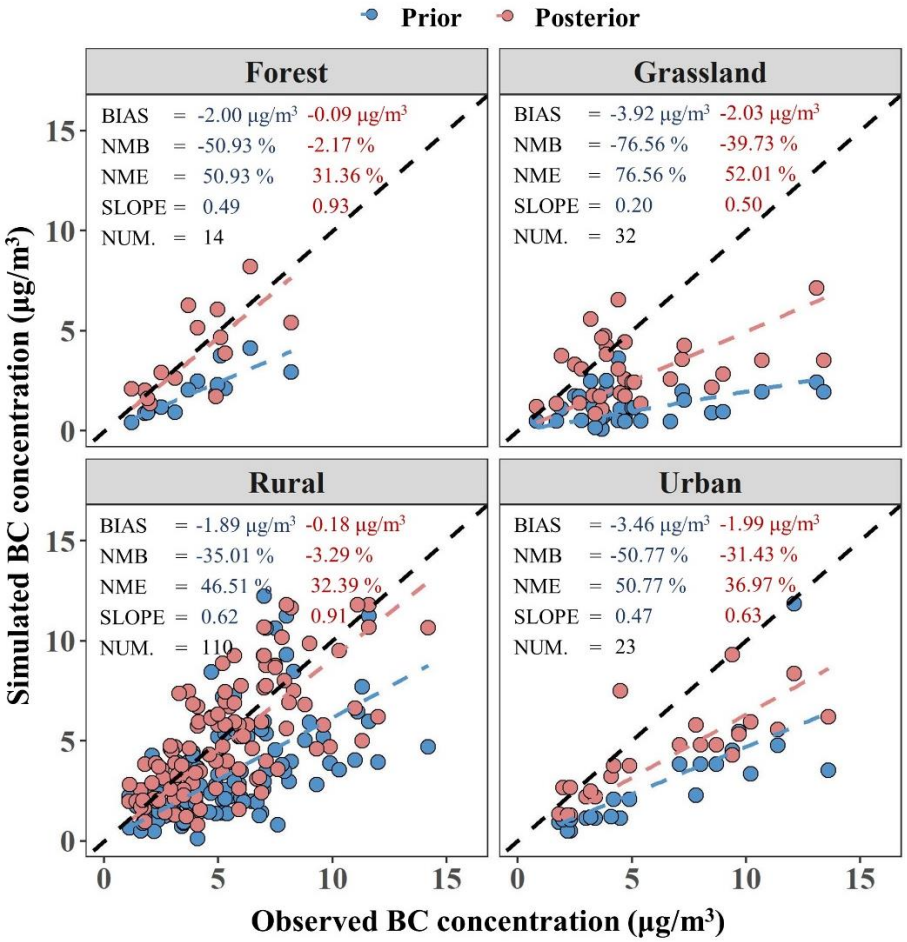

Note: The BIAS, NMB and NME were calculated using following equations (P and O indicate the results from model simulation and observation, respectively):

$$BIAS = \frac{1}{n}\sum_{i=1}^{n}(P_i - O_i)$$

$$NMB = \frac{\sum_{i=1}^{n}(P_i - O_i)}{\sum_{i=1}^{n} O_i} \times 100\%$$

$$NME = \frac{\sum_{i=1}^{n}|P_i - O_i|}{\sum_{i=1}^{n} O_i}$$

Figure S8 Spatial distribution of premature mortality attributable to the posterior BC exposure during 2000-2020 (with a five-year interval).

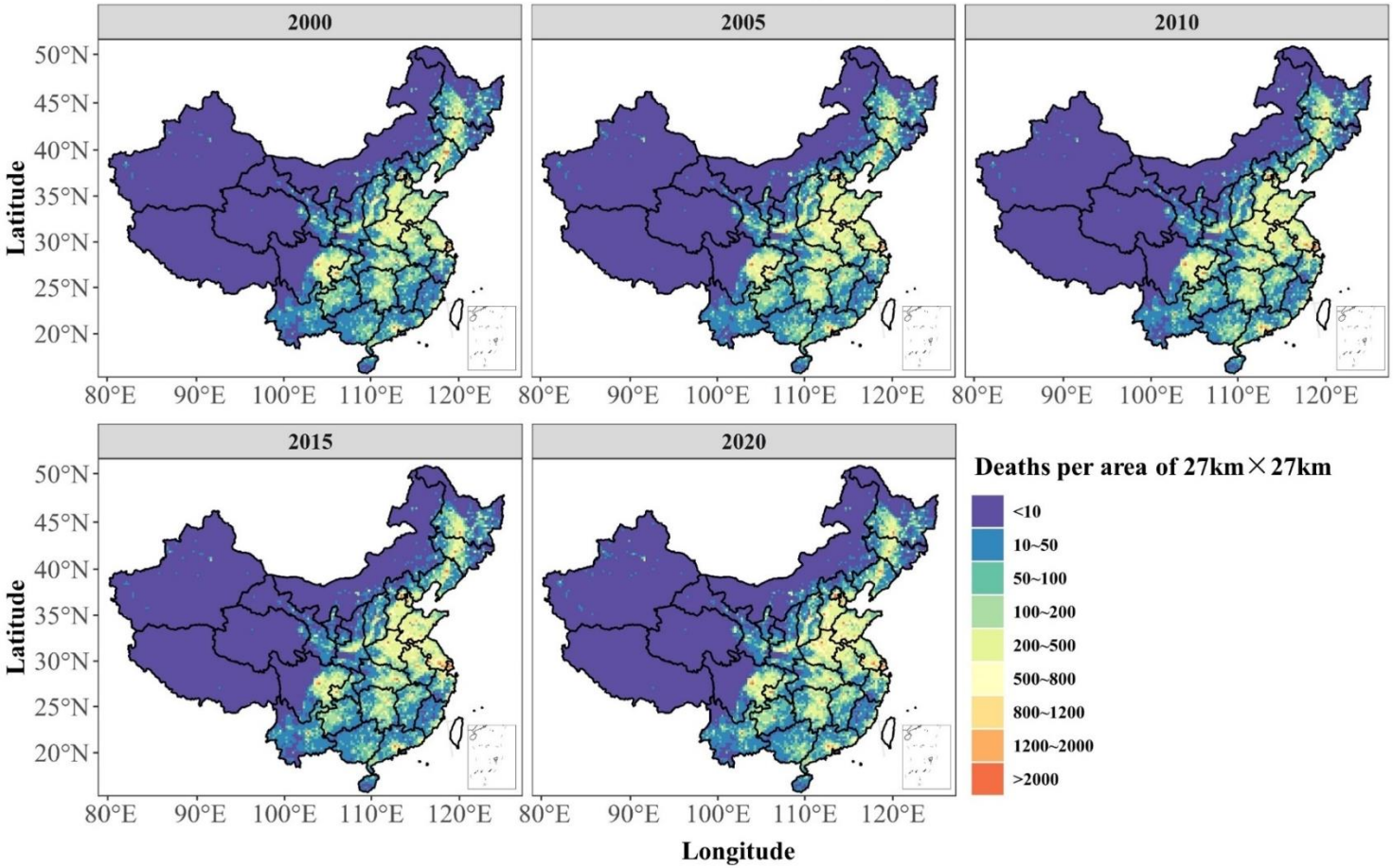

Figure S9 Annual average contribution of interannual meteorological variation to changes of BC concentration (compared with the starting year of each subplot). Unit: μg/m^3.

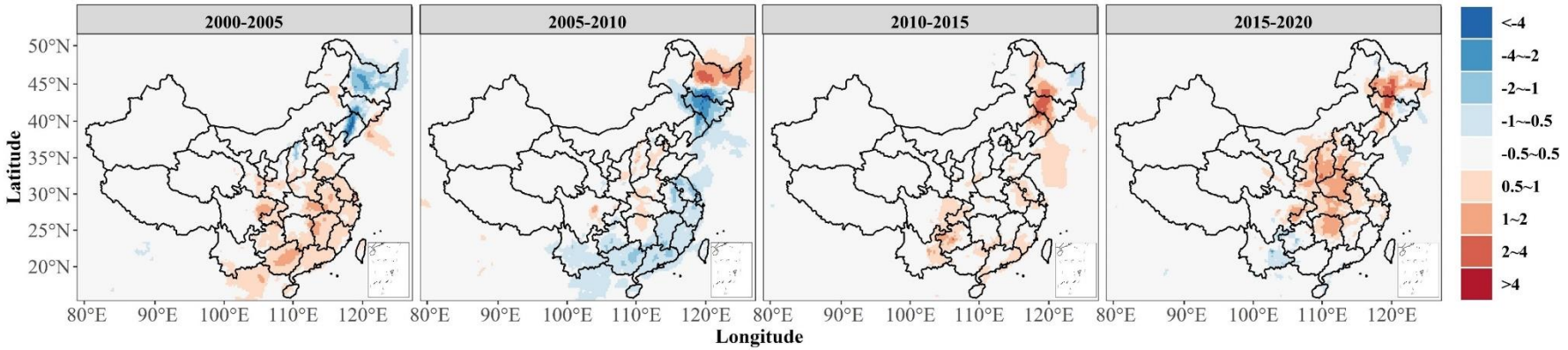

Figure S10 Multiyear average fractions of BC AAOD to AAOD from MERRA-2.

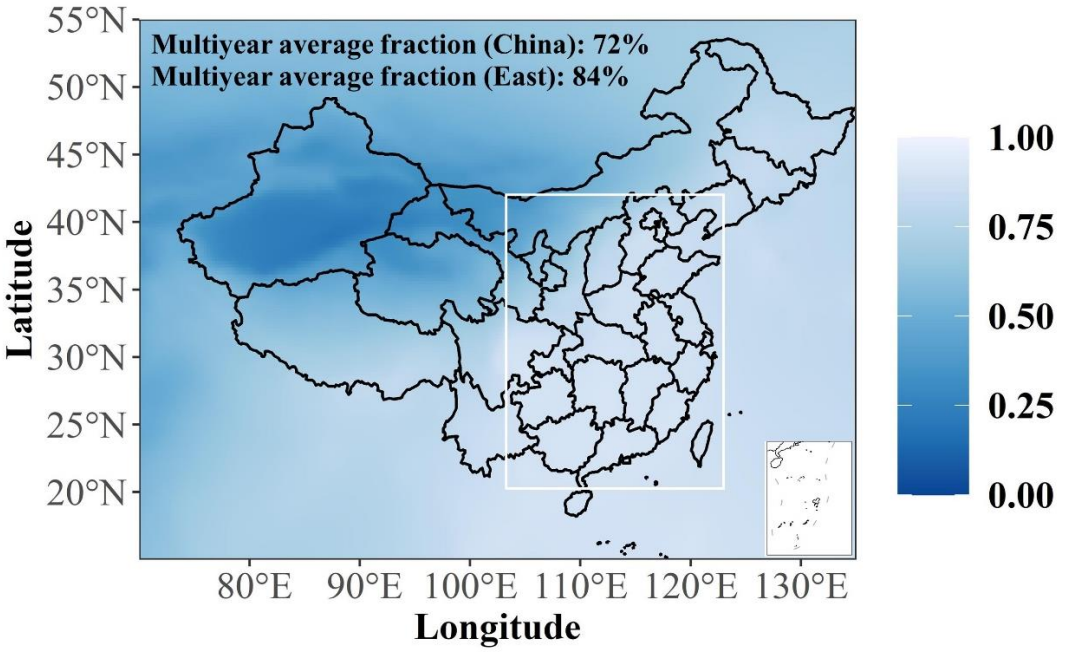

References

Bai, Z., Cui, X., Wang, X., Xie, H., and Chen, B.: Light absorption of black carbon is doubled at Mt. Tai and typical urban area in North China, Sci. Total Environ., 635, 1144-1151, https://doi.org/https://doi.org/10.1016/j.scitotenv.2018.04.244, 2018.

Bakatsoula, V. D., Korras-Carraca, M.-B., Hatzianastassiou, N., and Matsoukas, C.: A comparison of atmospheric aerosol absorption properties from the MERRA-2 reanalysis with AERONET, Atmos. Environ., 311, 119997, https://doi.org/https://doi.org/10.1016/j.atmosenv.2023.119997, 2023.

Binkowski, F. S. and Roselle, S. J.: Models-3 community multiscale air quality (CMAQ) model aerosol component - 1. Model description, J. Geophys. Res.-Atmos., 108, https://doi.org/10.1029/2001jd001409, 2003.

Bond, T. C., Doherty, S. J., Fahey, D. W., Forster, P. M., Berntsen, T., DeAngelo, B. J., Flanner, M. G., Ghan, S., Karcher, B., Koch, D., Kinne, S., Kondo, Y., Quinn, P. K., Sarofim, M. C., Schultz, M. G., Schulz, M., Venkataraman, C., Zhang, H., Zhang, S., Bellouin, N., Guttikunda, S. K., Hopke, P. K., Jacobson, M. Z., Kaiser, J. W., Klimont, Z., Lohmann, U., Schwarz, J. P., Shindell, D., Storelvmo, T., Warren, S. G., and Zender, C. S.: Bounding the role of black carbon in the climate system: A scientific assessment, J. Geophys. Res.-Atmos., 118, 5380-5552, https://doi.org/10.1002/jgrd.50171, 2013.

Buchard, V., Randles, C. A., da Silva, A. M., Darmenov, A., Colarco, P. R., Govindaraju, R., Ferrare, R., Hair, J., Beyersdorf, A. J., Ziemba, L. D., and Yu, H.: The MERRA-2 Aerosol Reanalysis, 1980 Onward. Part II: Evaluation and Case Studies, J. Clim., 30, 6851-6872, https://doi.org/10.1175/jcli-d-16-0613.1, 2017.

Cai, Z., Li, Z., Li, P., Li, J., Sun, H., Yang, Y., Gao, X., Ren, G., Ren, R., and Wei, J.: Vertical distributions of aerosol microphysical and optical properties based on aircraft measurements made over the Loess Plateau in China, Atmos. Environ., 270, 118888, https://doi.org/10.1016/j.atmosenv.2021.118888, 2022.

Cao, F., Zhang, X., Hao, C., Tiwari, S., and Chen, B.: Light absorption enhancement of particulate matters and their source apportionment over the Asian continental outflow site and South Yellow Sea, Environ. Sci. Pollut. Res., 28, 8022-8035, https://doi.org/10.1007/s11356-020-11134-y, 2021.

Chen, B., Bai, Z., Cui, X., Chen, J., Andersson, A., and Gustafsson, Ö.: Light absorption enhancement of black carbon from urban haze in Northern China winter, Environ.

Pollut., 221, 418-426, https://doi.org/https://doi.org/10.1016/j.envpol.2016.12.004, 2017a.

Chen, B., Zhu, Z. J., Wang, X. F., Andersson, A., Chen, J. M., Zhang, Q. Z., and Gustafsson, O.: Reconciling modeling with observations of radiative absorption of black carbon aerosols, J. Geophys. Res.-Atmos., 122, 5932-5942, https://doi.org/10.1002/2017jd026548, 2017b.

Chen, B., Du, K., Wang, Y., Chen, J., Zhao, J., Wang, K., Zhang, F., and Xu, L.: Emission and Transport of Carbonaceous Aerosols in Urbanized Coastal Areas in China, Aerosol Air Qual. Res., 12, 371-378, https://doi.org/10.4209/aaqr.2011.08.0131, 2012.

Chen, D., Zhao, Y., Lyu, R. T., Wu, R. R., Dai, L., Zhao, Y., Chen, F., Zhang, J., Yu, H., and Guan, M.: Seasonal and spatial variations of optical properties of light absorbing carbon and its influencing factors in a typical polluted city in Yangtze River Delta, China, Atmos. Environ., 199, 45-54, https://doi.org/10.1016/j.atmosenv.2018.11.022, 2019a.

Chen, P., Kang, S., Li, C., Zhang, Q., Guo, J., Tripathee, L., Zhang, Y., Li, G., Gul, C., Cong, Z., Wan, X., Niu, H., Panday, A. K., Rupakheti, M., and Ji, Z.: Carbonaceous aerosol characteristics on the Third Pole: A primary study based on the Atmospheric Pollution and Cryospheric Change (APCC) network, Environ. Pollut., 253, 49-60, https://doi.org/https://doi.org/10.1016/j.envpol.2019.06.112, 2019b.

Chen, W., Cao, X., Ran, H., Chen, T., Yang, B., and Zheng, X.: Concentration and source allocation of black carbon by AE-33 model in urban area of Shenzhen, southern China, J. Environ. Health. Sci. Eng., 20, 469-483, https://doi.org/10.1007/s40201-022-00793-3, 2022.

Chen, Y., Zhang, S., Peng, C., Shi, G., Tian, M., Huang, R. J., Guo, D., Wang, H., Yao, X., and Yang, F.: Impact of the COVID-19 pandemic and control measures on air quality and aerosol light absorption in Southwestern China, Sci. Total Environ., 749, 141419, https://doi.org/10.1016/j.scitotenv.2020.141419, 2020.

Chen, Y., Chen, R., Chen, Y., Dong, X., Zhu, J., Liu, C., van Donkelaar, A., Martin, R. V., Li, H., Kan, H., Jiang, Q., and Fu, C.: The prospective effects of long-term exposure to ambient PM2.5 and constituents on mortality in rural East China, Chemosphere, 280, 130740, https://doi.org/10.1016/j.chemosphere.2021.130740,

2021.

Cheng, H. R., Wang, Z. W., Feng, J. L., Chen, H. L., Zhang, F., and Liu, J.: Carbonaceous species composition and source apportionment of PM2.5 in urban atmosphere of Wuhan, Ecol. Evol. Sci., 21, 1574-1579 (in Chinese), 2012.

Cheng, Y., He, K. B., Zheng, M., Duan, F. K., Du, Z. Y., Ma, Y. L., Tan, J. H., Yang, F. M., Liu, J. M., Zhang, X. L., Weber, R. J., Bergin, M. H., and Russell, A. G.: Mass absorption efficiency of elemental carbon and water-soluble organic carbon in Beijing, China, Atmos. Chem. Phys., 11, 11497-11510, https://doi.org/10.5194/acp-11-11497-2011, 2011.

Cui, F., Pei, S., Chen, M., and Ma, Y.: Seasonal variation and source analyses of aerosol optical properties in Nanjing, China, Atmos. Pollut. Res., 12, 101117, https://doi.org/https://doi.org/10.1016/j.apr.2021.101117, 2021a.

Cui, S., Xian, J., Shen, F., Zhang, L., Deng, B., Zhang, Y., and Ge, X.: One-Year Real-Time Measurement of Black Carbon in the Rural Area of Qingdao, Northeastern China: Seasonal Variations, Meteorological Effects, and the COVID-19 Case Analysis, Atmosphere, 12, 394, https://doi.org/10.3390/atmos12030394, 2021b.

Cui, X., Wang, X., Yang, L., Chen, B., Chen, J., Andersson, A., and Gustafsson, Ö.: Radiative absorption enhancement from coatings on black carbon aerosols, Sci. Total Environ., 551-552, 51-56, https://doi.org/https://doi.org/10.1016/j.scitotenv.2016.02.026, 2016.

Ding, J., Huang, W., Zhao, J., Li, L., Xiong, G., Jiang, C., Ye, D., Li, D., Wang, J., Yu, J., and Liu, R.: Characteristics and source origins of carbonaceous aerosol in fine particulate matter in a megacity, Sichuan Basin, southwestern China, Atmos. Pollut. Res., 13, 101266, https://doi.org/10.1016/j.apr.2021.101266, 2022.

Ding, S., Liu, D. T., Hu, K., Zhao, D. L., Tian, P., Wang, F., Li, R. J., Chen, Y. C., He, H., Huang, M. Y., and Ding, D. P.: Optical and hygroscopic properties of black carbon influenced by particle microphysics at the top of the anthropogenically polluted boundary layer, Atmos. Chem. Phys., 21, 681-694, https://doi.org/10.5194/acp-21-681-2021, 2021.

Duan, F. K., He, K. B., Ma, Y. L., Yang, F. M., Yu, X. C., Cadle, S. H., Chan, T., and Mulawa, P. A.: Concentration and chemical characteristics of PM2.5 in Beijing, China: 2001-2002, Sci. Total Environ., 355, 264-275, https://doi.org/10.1016/j.scitotenv.2005.03.001, 2006.

Duan, J., Tan, J., Cheng, D., Bi, X., Deng, W., Sheng, G., Fu, J., and Wong, M. H.: Sources and characteristics of carbonaceous aerosol in two largest cities in Pearl River Delta Region, China, Atmos. Environ., 41, 2895-2903, https://doi.org/10.1016/j.atmosenv.2006.12.017, 2007.

Emery, C., Tai, E., and Yarwood, G.: Enhanced meteorological modeling and performance evaluation for two texas episodes, Report to the Texas Natural Resources Conservation Commission, the Texas Natural Resources Conservation Commission, ENVIRON, International Corp., Novato, CA, https://www.tceq.texas.gov/assets/public/implementation/air/am/contracts/reports/mm/EnhancedMetModelingAndPerformanceEvaluation.pdf, 2001.

Feng, Y., Chen, Y., Guo, H., Zhi, G., Xiong, S., Li, J., Sheng, G., and Fu, J.: Characteristics of organic and elemental carbon in PM2.5 samples in Shanghai, China, Atmos. Res., 92, 434-442, https://doi.org/10.1016/j.atmosres.2009.01.003, 2009.

Fu, X., Wang, X., Guo, H., Cheung, K. L., Ding, X., Zhao, X., He, Q., Gao, B., Zhang, Z., Liu, T., and Zhang, Y.: Trends of ambient fine particles and major chemical components in the Pearl River Delta region: Observation at a regional background site in fall and winter, Sci. Total Environ., 497, 274-281, https://doi.org/10.1016/j.scitotenv.2014.08.008, 2014.

Geng, G., Zheng, Y., Zhang, Q., Xue, T., Zhao, H., Tong, D., Zheng, B., Li, M., Liu, F., Hong, C., He, K., and Davis, S. J.: Drivers of PM2.5 air pollution deaths in China 2002–2017, Nat. Geosci., 14, 645–650, https://doi.org/10.1038/s41561-021-00792-3, 2021.

Geng, G. N., Zhang, Q., Tong, D., Li, M., Zheng, Y. X., Wang, S. W., and He, K. B.: Chemical composition of ambient PM2.5 over China and relationship to precursor emissions during 2005-2012, Atmos. Chem. Phys., 17, 9187-9203, https://doi.org/10.5194/acp-17-9187-2017, 2017.

Geng, N., Wang, J., Xu, Y., Zhang, W., Chen, C., and Zhang, R.: PM2.5 in an industrial district of Zhengzhou, China: Chemical composition and source apportionment, Particuology, 11, 99-109, https://doi.org/10.1016/j.partic.2012.08.004, 2013.

Gliß, J., Mortier, A., Schulz, M., Andrews, E., Balkanski, Y., Bauer, S. E., Benedictow, A. M. K., Bian, H., Checa-Garcia, R., Chin, M., Ginoux, P., Griesfeller, J. J., Heckel, A., Kipling, Z., Kirkevåg, A., Kokkola, H., Laj, P., Le Sager, P., Lund, M.

T., Lund Myhre, C., Matsui, H., Myhre, G., Neubauer, D., van Noije, T., North, P., Olivié, D. J. L., Rémy, S., Sogacheva, L., Takemura, T., Tsigaridis, K., and Tsyro, S. G.: AeroCom phase III multi-model evaluation of the aerosol life cycle and optical properties using ground- and space-based remote sensing as well as surface in situ observations, Atmos. Chem. Phys., 21, 87-128, https://doi.org/10.5194/acp-21-87-2021, 2021.

Gu, J., Bai, Z., Liu, A., Wu, L., Xie, Y., Li, W., Dong, H., and Zhang, X.: Characterization of Atmospheric Organic Carbon and Element Carbon of PM2.5 and PM10 at Tianjin, China, Aerosol Air Qual. Res., 10, 167-176, https://doi.org/10.4209/aaqr.2009.12.0080, 2010.

Gu, J., Du, S., Han, D., Hou, L., Yi, J., Xu, J., Liu, G., Han, B., Yang, G., and Bai, Z.-P.: Major chemical compositions, possible sources, and mass closure analysis of PM2.5 in Jinan, China, Air Qual. Atmos. Health, 7, 251-262, https://doi.org/10.1007/s11869-013-0232-9, 2014.

He, K. B., Yang, F. M., Ma, Y. L., Zhang, Q., Yao, X. H., Chan, C. K., Cadle, S., Chan, T., and Mulawa, P.: The characteristics of PM2.5 in Beijing, China, Atmos. Environ., 35, 4959-4970, https://doi.org/10.1016/s1352-2310(01)00301-6, 2001.

Hu, Z. F., Kang, S. C., Li, C. L., Yan, F. P., Chen, P. F., Gao, S. P., Wang, Z. Y., Zhang, Y. L., and Sillanpaa, M.: Light absorption of biomass burning and vehicle emission-sourced carbonaceous aerosols of the Tibetan Plateau, Environ. Sci. Pollut. Res., 24, 15369-15378, https://doi.org/10.1007/s11356-017-9077-3, 2017.

Huang, X., Yun, H., Gong, Z., Li, X., He, L., Zhang, Y., and Hu, M.: Source apportionment and secondary organic aerosol estimation of PM2.5 in an urban atmosphere in China, Sci China Earth Sci, 57, 1352-1362, https://doi.org/10.1007/s11430-013-4686-2, 2014.

Janssen, N. A., Hoek, G., Simic-Lawson, M., Fischer, P., van Bree, L., ten Brink, H., Keuken, M., Atkinson, R. W., Anderson, H. R., Brunekreef, B., and Cassee, F. R.: Black carbon as an additional indicator of the adverse health effects of airborne particles compared with PM10 and PM2.5, Environ. Health Perspect., 119, 1691-1699, https://doi.org/10.1289/ehp.1003369, 2011.

Ji, D. S., Li, L., Pang, B., Xue, P., Wang, L. L., Wu, Y. F., Zhang, H. L., and Wang, Y. S.: Characterization of black carbon in an urban-rural fringe area of Beijing, Environ. Pollut., 223, 524-534, https://doi.org/10.1016/j.envpol.2017.01.055,

2017.

Krewski, D., Jerrett, M., Burnett, R. T., Ma, R., Hughes, E., Shi, Y., Turner, M. C., Pope III, C. A., Thurston, G., and Calle, E. E.: Extended follow-up and spatial analysis of the American Cancer Society study linking particulate air pollution and mortality, Health Effects Institute Boston, MA, 2009.

Lan, Z.-J., Huang, X.-F., Yu, K.-Y., Sun, T.-L., Zeng, L.-W., and Hu, M.: Light absorption of black carbon aerosol and its enhancement by mixing state in an urban atmosphere in South China, Atmos. Environ., 69, 118-123, https://doi.org/https://doi.org/10.1016/j.atmosenv.2012.12.009, 2013.

Li, B., Zhang, J., Zhao, Y., Yuan, S., Zhao, Q., Shen, G., and Wu, H.: Seasonal variation of urban carbonaceous aerosols in a typical city Nanjing in Yangtze River Delta, China, Atmos. Environ., 106, 223-231, https://doi.org/10.1016/j.atmosenv.2015.01.064, 2015.

Li, J. J., Wang, G. H., Wang, X. M., Cao, J. J., Sun, T., Cheng, C. L., Meng, J. J., Hu, T. F., and Liu, S. X.: Abundance, composition and source of atmospheric PM2.5 at a remote site in the Tibetan Plateau, China, Tellus B: Chem. Phys. Meteorol., 65, 20281, https://doi.org/10.3402/tellusb.v65i0.20281, 2013.

Li, S., Zhu, M., Yang, W., Tang, M., Huang, X., Yu, Y., Fang, H., Yu, X., Yu, Q., Fu, X., Song, W., Zhang, Y., Bi, X., and Wang, X.: Filter-based measurement of light absorption by brown carbon in PM2.5 in a megacity in South China, Sci. Total Environ., 633, 1360-1369, https://doi.org/https://doi.org/10.1016/j.scitotenv.2018.03.235, 2018.

Li, W., Bai, Z., Liu, A., Chen, J., and Chen, L.: Characteristics of Major PM2.5 Components during Winter in Tianjin, China, Aerosol Air Qual. Res., 9, 105-119, 2009.

Li, Y., Du, A., Li, Z., Li, J., Chen, C., Sun, J., Qiu, Y., Zhang, Z., Wang, Q., Xu, W., Liu, X., Ji, D., Zhang, W., and Sun, Y.: Investigation of sources and formation mechanisms of fine particles and organic aerosols in cold season in Fenhe Plain, China, Atmos. Res., 268, 106018, https://doi.org/10.1016/j.atmosres.2022.106018, 2022.

Liang, F. C., Xiao, Q. Y., Huang, K. Y., Yang, X. L., Liu, F. C., Li, J. X., Lu, X. F., Liu, Y., and Gu, D. F.: The 17-y spatiotemporal trend of PM2.5 and its mortality burden in China, Proc. Natl. Acad. Sci. U.S.A., 117, 25601-25608,

https://doi.org/10.1073/pnas.1919641117, 2020.

Liu, B., Tan, X., Jin, Y., Yu, W., and Li, C.: Application of RR-XGBoost combined model in data calibration of micro air quality detector, Sci. Rep., 11, 15662, https://doi.org/10.1038/s41598-021-95027-1, 2021.

Liu, B., Li, T., Yang, J., Wu, J., Wang, J., Gao, J., Bi, X., Feng, Y., Zhang, Y., and Yang, H.: Source apportionment and a novel approach of estimating regional contributions to ambient PM2.5 in Haikou, China, Environ. Pollut., 223, 334-345, https://doi.org/10.1016/j.envpol.2017.01.030, 2017.

Liu, D., Li, J., Zhang, Y., Xu, Y., Liu, X., Ding, P., Shen, C., Chen, Y., Tian, C., and Zhang, G.: The Use of Levoglucosan and Radiocarbon for Source Apportionment of PM2.5 Carbonaceous Aerosols at a Background Site in East China, Environ. Sci. Technol., 47, 10454-10461, https://doi.org/10.1021/es401250k, 2013.

Liu, Y. J., Zhang, T. T., Liu, Q. Y., Zhang, R. J., Sun, Z. Q., and Zhang, M. G.: Seasonal Variation of Physical and Chemical Properties in TSP, PM10 and PM2.5 at a Roadside Site in Beijing and Their Influence on Atmospheric Visibility, Aerosol Air Qual. Res., 14, 954-969, https://doi.org/10.4209/aaqr.2013.01.0023, 2014.

Louie, P. K. K., Chow, J. C., Chen, L. W. A., Watson, J. G., Leung, G., and Sin, D. W. M.: PM2.5 chemical composition in Hong Kong: Urban and regional variations, Sci. Total Environ., 338, 267-281, https://doi.org/10.1016/j.scitotenv.2004.07.021, 2005a.

Louie, P. K. K., Watson, J. G., Chow, J. C., Chen, A., Sin, D. W. M., and Lau, A. K. H.: Seasonal characteristics and regional transport of PM2.5 in Hong Kong, Atmos. Environ., 39, 1695-1710, https://doi.org/10.1016/j.atmosenv.2004.11.017, 2005b.

Ma, Z. W., Dey, S., Christopher, S., Liu, R. Y., Bi, J., Balyan, P., and Liu, Y.: A review of statistical methods used for developing large-scale and long-term PM2.5 models from satellite data, Remote Sens. Environ., 269, 15, https://doi.org/10.1016/j.rse.2021.112827, 2022.

Meng, Z., Yang, P., Kattawar, G. W., Bi, L., Liou, K. N., and Laszlo, I.: Single-scattering properties of tri-axial ellipsoidal mineral dust aerosols: A database for application to radiative transfer calculations, J. Aerosol Sci., 41, 501-512, https://doi.org/https://doi.org/10.1016/j.jaerosci.2010.02.008, 2010.

Niu, H. W., Kang, S. C., Wang, H. L., Zhang, R. D., Lu, X. X., Qian, Y., Paudyal, R., Wang, S. J., Shi, X. F., and Yan, X. G.: Seasonal variation and light absorption

property of carbonaceous aerosol in a typical glacier region of the southeastern Tibetan Plateau, Atmos. Chem. Phys., 18, 6441-6460, https://doi.org/10.5194/acp-18-6441-2018, 2018.

Pathak, R. K., Wang, T., Ho, K. F., and Lee, S. C.: Characteristics of summertime PM2.5 organic and elemental carbon in four major Chinese cities: Implications of high acidity for water-soluble organic carbon (WSOC), Atmos. Environ., 45, 318-325, https://doi.org/10.1016/j.atmosenv.2010.10.021, 2011.

Pleim, J. and Ran, L.: Surface Flux Modeling for Air Quality Applications, Atmosphere, 2, 271-302, https://doi.org/10.3390/atmos2030271, 2011.

Shen, G., Xue, M., Yuan, S., Zhang, J., Zhao, Q., Li, B., Wu, H., and Ding, A.: Chemical compositions and reconstructed light extinction coefficients of particulate matter in a mega-city. in the western Yangtze River Delta, China, Atmos. Environ., 83, 14-20, https://doi.org/10.1016/j.atmosenv.2013.10.055, 2014.

Song, Y., Xie, S., Zhang, Y., Zeng, L., Salmon, L. G., and Zheng, M.: Source apportionment of PM2.5 in Beijing using principal component analysis/absolute principal component scores and UNMIX, Sci. Total Environ., 372, 278-286, https://doi.org/10.1016/j.scitotenv.2006.08.041, 2006.

Song, Y., Tang, X., Xie, S., Zhang, Y., Wei, Y., Zhang, M., Zeng, L., and Lu, S.: Source apportionment of PM2.5 in Beijing in 2004, J. Hazard. Mater., 146, 124-130, https://doi.org/10.1016/j.jhazmat.2006.11.058, 2007.

Sun, J. Y., Wu, C., Wu, D., Cheng, C., Li, M., Li, L., Deng, T., Yu, J. Z., Li, Y. J., Zhou, Q., Liang, Y., Sun, T., Song, L., Cheng, P., Yang, W., Pei, C., Chen, Y., Cen, Y., Nian, H., and Zhou, Z.: Amplification of black carbon light absorption induced by atmospheric aging: temporal variation at seasonal and diel scales in urban Guangzhou, Atmos. Chem. Phys., 20, 2445-2470, https://doi.org/10.5194/acp-20-2445-2020, 2020.

Tan, Y., Wang, H., Zhu, B., Zhao, T., Shi, S., Liu, A., Liu, D., Pan, C., and Cao, L.: The interaction between black carbon and planetary boundary layer in the Yangtze River Delta from 2015 to 2020: Why O3 didn't decline so significantly as PM2.5, Environ. Res., 214, 114095, https://doi.org/10.1016/j.envres.2022.114095, 2022.

Tang, X., Chen, X., and Tian, Y.: Chemical composition and source apportionment of PM2.5 - A case study from one year continuous sampling in the Chang-Zhu-Tan urban agglomeration, Atmos. Pollut. Res., 8, 885-899,

https://doi.org/10.1016/j.apr.2017.02.004, 2017.

Tao, J., Zhang, Z., Zhang, L., Wu, Y., Zhang, R., and Wang, B.: Impact of deliquescence of aerosol on mass absorption efficiency of elemental carbon in fine particles in urban Guangzhou in south China, Atmos. Environ., 256, 118476, https://doi.org/https://doi.org/10.1016/j.atmosenv.2021.118476, 2021.

Tao, J., Cheng, T., Zhang, R., Cao, J., Zhu, L., Wang, Q., Luo, L., and Zhang, L.: Chemical composition of PM2.5 at an urban site of Chengdu in southwestern China, Adv. Atmos. Sci., 30, 1070-1084, https://doi.org/10.1007/s00376-012-2168-7, 2013.

Tao, J., Zhang, L., Cao, J., Hsu, S.-C., Xia, X., Zhang, Z., Lin, Z., Cheng, T., and Zhang, R.: Characterization and source apportionment of aerosol light extinction in Chengdu, southwest China, Atmos. Environ., 95, 552-562, https://doi.org/https://doi.org/10.1016/j.atmosenv.2014.07.017, 2014a.

Tao, J., Gao, J., Zhang, L., Zhang, R., Che, H., Zhang, Z., Lin, Z., Jing, J., Cao, J., and Hsu, S. C.: PM2.5 pollution in a megacity of southwest China: source apportionment and implication, Atmos. Chem. Phys., 14, 8679-8699, https://doi.org/10.5194/acp-14-8679-2014, 2014b.

Tao, J., Zhang, L., Ho, K., Zhang, R., Lin, Z., Zhang, Z., Lin, M., Cao, J., Liu, S., and Wang, G.: Impact of PM2.5 chemical compositions on aerosol light scattering in Guangzhou - the largest megacity in South China, Atmos. Res., 135, 48-58, https://doi.org/10.1016/j.atmosres.2013.08.015, 2014c.

Tao, J., Zhang, L., Cao, J., Zhong, L., Chen, D., Yang, Y., Chen, D., Chen, L., Zhang, Z., Wu, Y., Xia, Y., Ye, S., and Zhang, R.: Source apportionment of PM2.5 at urban and suburban areas of the Pearl River Delta region, south China - With emphasis on ship emissions, Sci. Total Environ., 574, 1559-1570, https://doi.org/10.1016/j.scitotenv.2016.08.175, 2017.

Wang, P., Cao, J.-j., Shen, Z.-x., Han, Y.-m., Lee, S.-c., Huang, Y., Zhu, C.-s., Wang, Q.-y., Xu, H.-m., and Huang, R.-j.: Spatial and seasonal variations of PM2.5 mass and species during 2010 in Xi'an, China, Sci. Total Environ., 508, 477-487, https://doi.org/10.1016/j.scitotenv.2014.11.007, 2015.

Wang, Q., Jiang, N., Yin, S., Li, X., Yu, F., Guo, Y., and Zhang, R.: Carbonaceous species in PM2.5 and PM10 in urban area of Zhengzhou in China: Seasonal variations and source apportionment, Atmos. Res., 191, 1-11,

https://doi.org/10.1016/j.atmosres.2017.02.003, 2017a.

Wang, Q. L., Wang, L. L., Tao, M. H., Chen, N., Lei, Y. L., Sun, Y., Xin, J. Y., Li, T. T., Zhou, J. X., Liu, J. D., Ji, D. S., and Wang, Y. S.: Exploring the variation of black and brown carbon during COVID-19 lockdown in megacity Wuhan and its surrounding cities, China, Sci. Total Environ., 791, 148226, https://doi.org/10.1016/j.scitotenv.2021.148226, 2021.

Wang, Q. Y., Huang, R. J., Zhao, Z. Z., Cao, J. J., Ni, H. Y., Tie, X. X., Zhu, C. S., Shen, Z. X., Wang, M., Dai, W. T., Han, Y. M., Zhang, N. N., and Prevot, A. S. H.: Effects of photochemical oxidation on the mixing state and light absorption of black carbon in the urban atmosphere of China, Environ. Res. Lett., 12, 044012, https://doi.org/10.1088/1748-9326/aa64ea, 2017b.

Wei, X., Bi, X. H., Dong, H. Y., Chen, K., Sun, R., and Feng, Y. C.: Characteristics and Sources of Particulate Matter during Hazy and Non-Hazy Episodes in Tianjin City in Summer, Research of Environmental Sciences, 25, 1193-1200 (in Chinese), 2012.

Wu, C., Wu, D., and Yu, J. Z.: Quantifying black carbon light absorption enhancement with a novel statistical approach, Atmos. Chem. Phys., 18, 289-309, https://doi.org/10.5194/acp-18-289-2018, 2018a.

Wu, D., Wu, C., Liao, B., Chen, H., Wu, M., Li, F., Tan, H., Deng, T., Li, H., Jiang, D., and Yu, J. Z.: Black carbon over the South China Sea and in various continental locations in South China, Atmos. Chem. Phys., 13, 12257-12270, https://doi.org/10.5194/acp-13-12257-2013, 2013.

Wu, X. Q., Liu, J., Wu, Y. F., Wang, X., Yu, X. W., Shi, J. S., Bi, J. R., Huang, Z. W., Zhou, T., and Zhang, R. J.: Aerosol optical absorption coefficients at a rural site in Northwest China: The great contribution of dust particles, Atmos. Environ., 189, 145-152, https://doi.org/10.1016/j.atmosenv.2018.07.002, 2018b.

Xia, Y., Wu, Y., Guo, Z., Zhang, J., Xiao, X., Song, L., and Zhang, R.: Observational study on aerosol adsorption at a rural site in Northern China, China Powder Science and Technology, 23, 17-23 (in Chinese), 2017.

Xiao, Q. Y., Chang, H. H., Geng, G. N., and Liu, Y.: An Ensemble Machine-Learning Model To Predict Historical PM2.5 Concentrations in China from Satellite Data, Environ. Sci. Technol., 52, 13260-13269, https://doi.org/10.1021/acs.est.8b02917, 2018a.

Xiao, S., Yu, X., Zhu, B., He, J., Lv, R., and Sha, D.: Source Apportionment of Black Carbon Aerosol in the North Suburbn of Nanjing, Environmental Science, 39, 9-17 (in Chinese), 2018b.

Xie, C. H., Xu, W. Q., Wang, J. F., Wang, Q. Q., Liu, D. T., Tang, G. Q., Chen, P., Du, W., Zhao, J., Zhang, Y. J., Zhou, W., Han, T. T., Bian, Q. Y., Li, J., Fu, P. Q., Wang, Z. F., Ge, X. L., Allan, J., Coe, H., and Sun, Y. L.: Vertical characterization of aerosol optical properties and brown carbon in winter in urban Beijing, China, Atmos. Chem. Phys., 19, 165-179, https://doi.org/10.5194/acp-19-165-2019, 2019.

Xie, F., Lin, Y. C., Ren, L., Gul, C., Wang, J. Q., Cao, F., Zhang, Y. X., Xie, T., Wu, J. Y., and Zhang, Y. L.: Decrease of atmospheric black carbon and CO(2) concentrations due to COVID-19 lockdown at the Mt. Waliguan WMO/GAW baseline station in China, Environ. Res., 211, 112984, https://doi.org/10.1016/j.envres.2022.112984, 2022.

Xing, Z. Y., Deng, J. J., Mu, C., Wang, Y., and Du, K.: Seasonal Variation of Mass Absorption Efficiency of Elemental Carbon in the Four Major Emission Areas in China, Aerosol Air Qual. Res., 14, 1897-1905, https://doi.org/10.4209/aaqr.2014.06.0121, 2014.

Xu, J., Jia, C., He, J., Xu, H., Tang, Y. T., Ji, D., Yu, H., Xiao, H., and Wang, C.: Biomass burning and fungal spores as sources of fine aerosols in Yangtze River Delta, China - Using multiple organic tracers to understand variability, correlations and origins, Environ. Pollut., 251, 155-165, https://doi.org/10.1016/j.envpol.2019.04.090, 2019.

Xu, X., Qin, N., Qi, L., Zou, B., Cao, S., Zhang, K., Yang, Z., Liu, Y., Zhang, Y., and Duan, X.: Development of season-dependent land use regression models to estimate BC and PM1 exposure, Sci. Total Environ., 793, 148540, https://doi.org/10.1016/j.scitotenv.2021.148540, 2021.

Yang, F., He, K., Ye, B., Chen, X., Cha, L., Cadle, S. H., Chan, T., and Mulawa, P. A.: One-year record of organic and elemental carbon in fine particles in downtown Beijing and Shanghai, Atmos. Chem. Phys., 5, 1449-1457, https://doi.org/10.5194/acp-5-1449-2005, 2005a.

Yang, F., Tan, J., Zhao, Q., Du, Z., He, K., Ma, Y., Duan, F., Chen, G., and Zhao, Q.: Characteristics of PM2.5 speciation in representative megacities and across China, Atmos. Chem. Phys., 11, 5207-5219, https://doi.org/10.5194/acp-11-5207-2011,

2011.

Yang, H., Yu, J. Z., Ho, S. S. H., Xu, J. H., Wu, W. S., Wan, C. H., Wang, X. D., Wang, X. R., and Wang, L. S.: The chemical composition of inorganic and carbonaceous materials in PM2.5 in Nanjing, China, Atmos. Environ., 39, 3735-3749, https://doi.org/10.1016/j.atmosenv.2005.03.010, 2005b.

Yang, J., Zhao, Y., Cao, J., and Nielsen, C. P.: Co-benefits of carbon and pollution control policies on air quality and health till 2030 in China, Environ. Int., 152, 106482, https://doi.org/10.1016/j.envint.2021.106482, 2021.

Yang, L., Zhou, X., Wang, Z., Zhou, Y., Cheng, S., Xu, P., Gao, X., Nie, W., Wang, X., and Wang, W.: Airborne fine particulate pollution in Jinan, China: Concentrations, chemical compositions and influence on visibility impairment, Atmos. Environ., 55, 506-514, https://doi.org/10.1016/j.atmosenv.2012.02.029, 2012.

Yau, P. S., Lee, S. C., Cheng, Y., Huang, Y., Lai, S. C., and Xu, X. H.: Contribution of ship emissions to the fine particulate in the community near an international port in Hong Kong, Atmos. Res., 124, 61-72, https://doi.org/10.1016/j.atmosres.2012.12.009, 2013.

Ye, B. M., Ji, X. L., Yang, H. Z., Yao, X. H., Chan, C. K., Cadle, S. H., Chan, T., and Mulawa, P. A.: Concentration and chemical composition of PM2.5 in Shanghai for a 1-year period, Atmos. Environ., 37, 499-510, https://doi.org/10.1016/s1352-2310(02)00918-4, 2003.

Ye, Z., Liu, J., Gu, A., Feng, F., Liu, Y., Bi, C., Xu, J., Li, L., Chen, H., Chen, Y., Dai, L., Zhou, Q., and Ge, X.: Chemical characterization of fine particulate matter in Changzhou, China, and source apportionment with offline aerosol mass spectrometry, Atmos. Chem. Phys., 17, 2573-2592, https://doi.org/10.5194/acp-17-2573-2017, 2017.

Zhang, B. S. and Zhang, W. T.: Source apportionment of PM2.5 in ambient air of Baotou, Environmental Engineering, 32, 71-74 (in Chinese), https://doi.org/10.13205/j.hjgc.201404017, 2014.

Zhang, F., Zhao, J., Chen, J., Xu, Y., and Xu, L.: Pollution characteristics of organic and elemental carbon in PM2.5 in Xiamen, China, J. Environ. Sci., 23, 1342-1349, https://doi.org/10.1016/s1001-0742(10)60559-1, 2011.

Zhang, F., Xu, L., Chen, J., Yu, Y., Niu, Z., and Yin, L.: Chemical compositions and extinction coefficients of PM2.5 in peri-urban of Xiamen, China, during June

2009-May 2010, Atmos. Res., 106, 150-158, https://doi.org/10.1016/j.atmosres.2011.12.005, 2012.

Zhang, Q., Shen, Z. X., Lei, Y. L., Zhang, T., Zeng, Y. L., Ning, Z., Sun, J., Westerdahl, D., Xu, H. M., Wang, Q. Y., Cao, J. J., and Zhang, R. J.: Optical properties and source identification of black carbon and brown carbon: comparison of winter and summer haze episodes in Xi'an, Northwest China, Environ. Sci. Processes Impacts, 21, 2058-2069, https://doi.org/10.1039/c9em00320g, 2019.

Zhang, R., Jing, J., Tao, J., Hsu, S. C., Wang, G., Cao, J., Lee, C. S. L., Zhu, L., Chen, Z., Zhao, Y., and Shen, Z.: Chemical characterization and source apportionment of PM2.5 in Beijing: seasonal perspective, Atmos. Chem. Phys., 13, 7053-7074, https://doi.org/10.5194/acp-13-7053-2013, 2013.

Zhang, X. Y., Wang, Y. Q., Zhang, X. C., Guo, W., and Gong, S. L.: Carbonaceous aerosol composition over various regions of China during 2006, J. Geophys. Res., 113, D14111, https://doi.org/10.1029/2007jd009525, 2008.

Zhang, Y. and Kang, S.: Characteristics of carbonaceous aerosols analyzed using a multiwavelength thermal/optical carbon analyzer: A case study in Lanzhou City, Sci China Earth Sci, 62, 389-402, https://doi.org/10.1007/s11430-017-9245-9, 2019.

Zhang, Y. T., Liu, H., Lei, S. D., Xu, W. Y., Tian, Y., Yao, W. J., Liu, X. Y., Liao, Q., Li, J., Chen, C., Sun, Y. L., Fu, P. Q., Xin, J. Y., Cao, J. J., Pan, X. L., and Wang, Z. F.: Mixing state of refractory black carbon in fog and haze at rural sites in winter on the North China Plain, Atmos. Chem. Phys., 21, 17631-17648, https://doi.org/10.5194/acp-21-17631-2021, 2021.

Zhao, D., Huang, M., Tian, P., He, H., Lowe, D., Zhou, W., Sheng, J., Wang, F., Bi, K., Kong, S., Yang, Y., Liu, Q., Liu, D., and Ding, D.: Vertical characteristics of black carbon physical properties over Beijing region in warm and cold seasons, Atmos. Environ., 213, 296-310, https://doi.org/https://doi.org/10.1016/j.atmosenv.2019.06.007, 2019a.

Zhao, M., Huang, Z., Qiao, T., Zhang, Y., Xiu, G., and Yu, J.: Chemical characterization, the transport pathways and potential sources of PM2.5 in Shanghai: Seasonal variations, Atmos. Res., 158, 66-78, https://doi.org/10.1016/j.atmosres.2015.02.003, 2015a.

Zhao, M., Qiao, T., Huang, Z., Zhu, M., Xu, W., Xiu, G., Tao, J., and Lee, S.:

Comparison of ionic and carbonaceous compositions of PM2.5 in 2009 and 2012 in Shanghai, China, Sci. Total Environ., 536, 695-703, https://doi.org/10.1016/j.scitotenv.2015.07.100, 2015b.

Zhao, P. S., Dong, F., He, D., Zhao, X. J., Zhang, X. L., Zhang, W. Z., Yao, Q., and Liu, H. Y.: Characteristics of concentrations and chemical compositions for PM2.5 in the region of Beijing, Tianjin, and Hebei, China, Atmos. Chem. Phys., 13, 4631-4644, https://doi.org/10.5194/acp-13-4631-2013, 2013.

Zhao, Z., Cao, J., Chow, J. C., Watson, J. G., Chen, A. L. W., Wang, X., Wang, Q., Tian, J., Shen, Z., Zhu, C., Liu, S., Tao, J., Ye, Z., Zhang, T., Zhou, J., and Tian, R.: Multi-wavelength light absorption of black and brown carbon at a high-altitude site on the Southeastern margin of the Tibetan Plateau, China, Atmos. Environ., 212, 54-64, https://doi.org/https://doi.org/10.1016/j.atmosenv.2019.05.035, 2019b.

Zheng, C., Li, Z., Zhang, X., Jiang, H., and Zhou, X.: Seasonal Variation in Chemical Composition of Total Suspended Particles During the COVID-19 Pandemic in the Source Area of Urumqi River, Tianshan, China, Front. Earth Sci., 10, 859203, https://doi.org/10.3389/feart.2022.859203, 2022.